PERGAMON

Journal of Structural Geology 25 (2003) 1121–1139

JOURNAL OF STRUCTURAL GEOLOGY

www.elsevier.com/locate/jsg

Analysis of folding by superposition of strain patterns

F. Bastida[a,*], N.C. Bobillo-Ares[b], J. Aller[a], N.C. Toimil[a]

[a]*Departamento de Geología, Universidad de Oviedo, 33005-Oviedo, Spain*
[b]*Departamento de Matemáticas, Universidad de Oviedo, 33005-Oviedo, Spain*

Received 11 October 2001; revised 24 July 2002; accepted 24 July 2002

Abstract

Two methods have been developed in this paper to model the strain state and the layer geometry of folds. These methods analyse the superposition of strain patterns due to layer shortening, tangential longitudinal strain, flexural-flow and fold flattening. The first method multiplies the deformation gradients of these strain patterns to model the successive superposition of mechanisms. The second method is more general and is based on the transformation of points from the initial configuration to deformed points according to the geometrical properties of the folding mechanisms involved. This method simulates the simultaneous and successive superposition of strain patterns. Both methods generate graphic outputs that describe the strain variation through the folded layer. Another application of these methods is to attempt to find theoretical folds that fit natural or experimental folds and to perform a geometric and kinematical analysis of these folds. Knowledge of the shape of the folded layer and the cleavage pattern is the most common basic information available in natural folds that can be used to perform the analysis. Additional strain data from the folded rocks are valuable for improving knowledge of the kinematical mechanisms involved in the folding.

Keywords: Folding; Strain; Mathematical modelling; Cleavage

1. Introduction

Folds are common structures in nature and are typical structures originated by ductile deformation at all scales. The geometry and degree of evolution of these structures can be used as indicators of the amount of deformation undergone by rocks and their study can be the basis of valuable contributions to the determination of the displacement and strain patterns involved in the development of an orogen. Nevertheless, despite the interest that the study of folds presents, the determination of the kinematical folding mechanisms that operated in a given fold and its state of strain is a difficult problem to solve at present.

Many of the studies on folding have focused on the mechanics of the process and have tried to relate the forces or stresses driving the folding with geometrical features of the folded layers and the rheological properties of the materials involved. Hence, concepts such as dominant wavelength, amplification and selectivity of the folding (Biot, 1961, 1965) have been very useful to understanding the buckling process. However, these studies have some limitations as a result of the mathematical difficulty inherent in analysing relevant folding models and the added difficulty of verifying the results of the theoretical studies using natural folds, due to the limitations imposed by outcrops and the limitations in determining the rheological behaviour of the rocks during folding. On the other hand, the introduction of mathematical simplifying assumptions limits the validity of the theoretical results. Many of the results of buckling theory, for instance, can only be successfully applied to small fold amplitudes. For these reasons, studies aimed at confirming the mechanical theory of folding using natural examples are rare.

A different approach to the analysis of folding can be made from a purely geometrical perspective. In this method, available theoretical, experimental and field data about the geometry, strain patterns and other structural features of the folded layers can be used to construct models that describe their strain distribution. This analysis is independent of the stresses driving the folding or the rheological properties of rocks and it does not provide any direct knowledge about the causes that produced the folding, but it is a very useful tool to determine the geometry and kinematics of orogens and it constitutes a necessary basis for subsequent mechanical studies. In addition, this analysis does not require the

* Corresponding author.
E-mail address: bastida@geol.uniovi.es (F. Bastida).

0191-8141/03/$ - see front matter © 2002 Elsevier Science Ltd. All rights reserved.
PII: S0191-8141(02)00129-3

outcrops to be of as high a quality as mechanical analysis, since it can be made using individual layers and fold limbs.

The analysis of folds in the field, and the experimental and numerical studies of fold development, indicate that different mechanisms accommodate strain in the folded layers (layer shortening, shearing parallel to layer boundaries, tangential longitudinal strain, flattening, etc.). Ramsay (1967, pp. 391–456) established the basis of the strain analysis of folds and made important contributions to the knowledge of the main folding mechanisms. Subsequently, Hobbs (1971) analysed the strain in folded layers using transformation equations suitable for generating the forms of common folds. Treagus (1982) proposed a fold classification that relates the isogons and cleavage geometry, and studied some simple cases of strain distribution in folded layers. An excellent synthesis on folding mechanisms was made by Ramsay and Huber (1987, pp. 445–473), who made a detailed analysis of several situations with initial deformation of the layer combined with flexural-flow. Twiss and Moores (1992, pp. 314–321) show graphical examples of strain patterns resulting from several combinations of kinematical folding mechanisms. Hudleston et al. (1996) have discussed the occurrence of flexural flow in natural folds. Bobillo-Ares et al. (2000) have studied the properties of tangential longitudinal strain patterns. Ramsay and Lisle (2000) have made an analysis of the heterogeneous strain described by transformation equations that define similar fold forms and involve characteristic displacement patterns of shear folds and flattened shear folds.

These studies have provided important knowledge on individual folding mechanisms. Nevertheless, the actual mechanisms operating in natural folds are usually combinations of several single mechanisms, and have been studied in many cases from field observations, microfabric analysis or strain analysis. Certain of these studies have considered some of the folding mechanisms analysed in this paper (Chapple and Spang, 1974; Groshong, 1975; Hudleston and Holst, 1984; Hudleston and Srivastava, 1997; Gutiérrez-Alonso and Gross, 1999; among others), while many have focused on fault-related folds (Fisher and Anastasio, 1994; Anastasio et al., 1997; Erslev and Mayborn, 1997; Tavarnelli, 1997; Thorbjornsen and Dunne, 1997; Fischer and Jackson, 1999; among others). However, the analysis of kinematical folding mechanisms is in general a difficult task. The geometrical classifications of folded layers and surfaces, such as Ramsay's classification, for instance, are a good starting point for this analysis, but they are hardly used. The measurement of strain at many points within a folded layer is necessary for this analysis, but, unfortunately, it is a very difficult and time-consuming task. To perform the kinematical analysis of a folded layer, we must take advantage of all the information supplied by the geometry of the fold and the associated structures. In this regard, tectonic foliation is a basic structure that maintains a well-defined geometrical relationship with the associated folds and the strain ellipsoid. Overlooking the academic discussion about the exact orientation of slaty cleavage with respect to the strain ellipsoid, the perpendicularity between the tectonic primary foliation and the minor axis of the finite strain ellipsoid can be taken as a good approximation in most cases.

In accordance with the notion presented above, the present paper describes a method to construct, using combinations of the main kinematical folding mechanisms, theoretical fold models that contain all the information about the geometry and strain distribution in the folded layer. A theoretical fold is constructed by a succession of folding steps, where each step involves the application of a specific kinematical mechanism. The analysis is made on fold profiles assuming plane strain, and the results are presented in graphic form.

The method can also be used to analyse strain patterns in natural folds and to gain insight into the folding mechanisms that operated in their development. To conduct this analysis, the direction of the intersection between the cleavage surface and the profile plane of the natural fold is assumed to give the direction of the major axis of the strain ellipse.

The combination of strain patterns used in the theoretical models mainly involves layer shortening, flexural-flow, tangential longitudinal strain and fold flattening. The term 'layer shortening' is used with the meaning given by Ramberg (1964) and the terms 'flexural-flow' and 'tangential longitudinal strain' are used following the definition given by Ramsay (1967, pp. 391–403). The term 'fold flattening' is used to refer to a superposition on a previous fold of a homogeneous irrotational strain with the direction of maximum shortening normal to the axial surface (see, for instance, Ramsay, 1962, 1967, pp. 411–415; Twiss and Moores, 1992, p. 319). Layer shortening and fold flattening are both a homogeneous strain superposed to the folds, but their effects on the fold geometry are different. The former occurs in the early stages of folding, whereas the latter occurs in the late stages.

The method also enables the introduction of homogeneous strain with maximum shortening perpendicular to the original configuration of the layer, simulating compaction prior to the folding (Ramsay and Huber, 1987, p. 447), or longitudinal to the axial surface, simulating a strain subsequent to the folding and giving rise to unfolding of the layer. These strains involve the same mathematical transformation as the other homogeneous strain patterns.

This paper provides insight into the kinematical analysis of natural folded layers by comparison with theoretical fold models. The analysis is mainly applicable to symmetrical folds, although it may give good results in folds with low asymmetry. The analysis unit is generally a single limb of a folded layer. The definition of fold limb is taken from Bastida et al. (1999) and is applied to the folded configuration of the original midway line between the layer boundaries, termed the 'guideline' (GL). The strain patterns considered are combined and analysed as the result

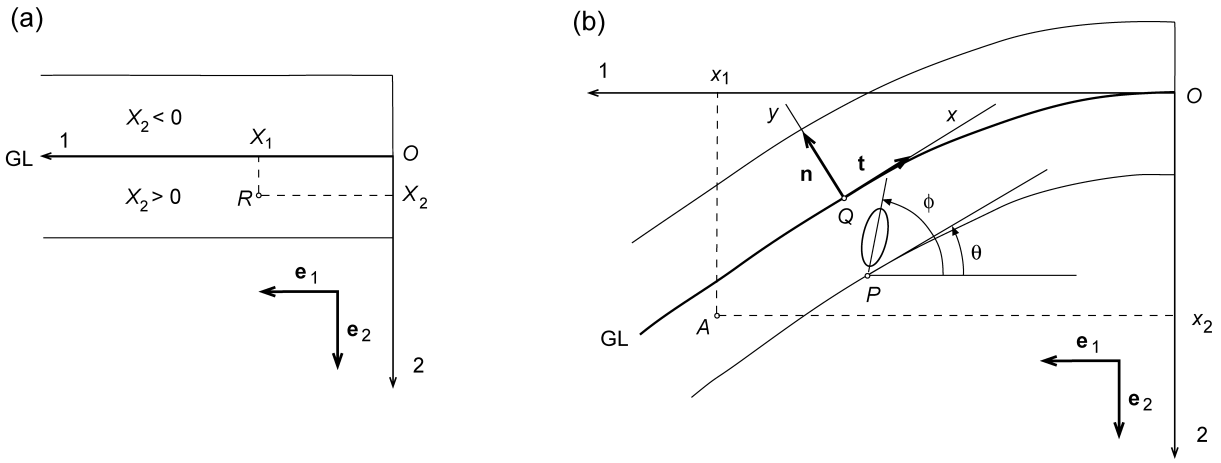

Fig. 1. (a) Initial configuration of the layer showing the reference system used ($\mathbf{e}_1$, $\mathbf{e}_2$) in the analysis. (b) General ($\mathbf{e}_1$, $\mathbf{e}_2$) and local ($\mathbf{t}$, $\mathbf{n}$) reference systems used for strain analysis of a folded layer and angular parameters used to describe the strain pattern; θ is the layer dip in P, and ϕ gives the orientation of the major axis of the finite strain ellipse at the same point. GL is the guideline.

of successive or simultaneous superpositions. The latter involves a more general analysis in which the models of successive superpositions are particular cases. Nevertheless, successive superposition is mathematically simpler and yields some relevant cases; for this reason, it will be considered first.

2. Successive superposition of deformations in folding

The general material deformation gradients ($\mathbf{F}$ and $\mathbf{F}'$) of the successive superposition of: (a) layer shortening, (b) flexural-flow, (c) tangential longitudinal strain, and (d) flattening, are given by:

$$\mathbf{F} = \mathbf{F}_F\mathbf{F}_S\mathbf{F}_T\mathbf{F}_{Sh}, \tag{1}$$

and

$$\mathbf{F}' = \mathbf{F}_F\mathbf{F}_T\mathbf{F}_S\mathbf{F}_{Sh}, \tag{2}$$

where $\mathbf{F}_F$, $\mathbf{F}_S$, $\mathbf{F}_T$ and $\mathbf{F}_{Sh}$ are the material deformation gradients of flattening, flexural-flow, tangential longitudinal strain and layer shortening, respectively. Eqs. (1) and (2) differ in the order of application of gradients $\mathbf{F}_S$ and $\mathbf{F}_T$. This change in order gives rise to different final results due to the non-commutative character of the matrix product. Another notable point about Eqs. (1) and (2) is that the factors are written in reverse order to that of the physical successive application of the deformations. In these equations, the application of a specific mechanism can be cancelled by making the corresponding matrix to be a unit matrix. Since $\mathbf{F}_F$ and $\mathbf{F}_{Sh}$ represent homogeneous strain, $\mathbf{F}_S$ or $\mathbf{F}_T$ must not be unit matrices for folding to occur. In this part of the paper we analyse a few simple cases of superposition of the deformation gradients to model folds. More complicated cases of superposition of strain patterns will be analysed below by the development of a more general model.

The general reference system for the analysis of the deformation at any point of the layer profile has its origin at the hinge point and is defined by base vectors $\mathbf{e}_1$ and $\mathbf{e}_2$, the latter in the inward direction of the axial trace and the former perpendicular to it (Fig. 1); the coordinates of any point A will be denoted as (x_1, x_2). To define lengths and coordinate values, the original arc length of the GL in a fold limb will be taken as the measure unit. Dip zero corresponds to that of the 1-axis, and the convention for the sign of the layer dip θ is given in Fig. 1. The orientation of the principal direction $\mathbf{m}^{(1)}$, corresponding to the principal strain value λ_1', is given by the angle ϕ (measured between 0 and 180°), as shown in Fig. 1.

Two types of graphs will be used to illustrate the results of the analysis. The first one describes the variation in ϕ as a function of the layer dip θ, and the second one describes the variation in the aspect ratio of the finite strain ellipse (ratio between axes, $R = \sqrt{\lambda_1'/\lambda_2'}$) as a function of the layer dip. To interpret the first type of graph, the terminology of cleavage patterns is used. Therefore, in a limb with positive dip, the orientation of $\mathbf{m}^{(1)}$ is an axial plane pattern when $\phi = 90°$, a convergent fan when $\phi > 90°$, and a divergent fan when $\phi < 90°$. A mixed pattern is frequent, sometimes involving the existence of a minimum or maximum in the ϕ vs. θ curve. In order to indicate the area of more probable cleavage development, in both types of graphs the part of the curves with $R \geq 2$ (corresponding to a shortening of about 30% when there is no area change) has been enhanced. The appearance of primary cleavage depends on the rheological behaviour of the rock and other factors, but is common with this R value.

2.1. Obtaining the principal direction $\mathbf{m}^{(1)}$

From the material deformation gradient of a superposition of deformations [e.g. $\mathbf{F}$ from Eq. (1)], the spatial

deformation gradient is given by:

$$\mathbf{f} = \mathbf{F}^{-1} = \begin{bmatrix} \frac{F_{22}}{\det F} & \frac{-F_{12}}{\det F} \\ \frac{-F_{21}}{\det F} & \frac{F_{11}}{\det F} \end{bmatrix} = \left[f_{ij}\right] \tag{3}$$

where $\det F = F_{11}F_{22} - F_{12}F_{21}$. When no area change is assumed, $\det F = 1$.

Cauchy's finite strain tensor of the superposition is:

$$\mathbf{c} = \mathbf{f}^{\mathrm{T}}\mathbf{f} = \left[c_{ij}\right], \tag{4}$$

where $\mathbf{f}^{\mathrm{T}}$ is the transposed matrix of $\mathbf{f}$.

The invariants of $\mathbf{c}$ are:

$$i_1 = c_{11} + c_{22} \qquad \text{and} \qquad i_2 = c_{11}c_{22} - c_{12}^2, \tag{5}$$

and the principal values, λ_1' and λ_2', are the roots of the equation:

$$\lambda'^2 - i_1\lambda' + i_2 = 0. \tag{6}$$

Taking as unity the second component of an eigenvector $\mathbf{m}^{(1)}$ ($m_2^{(1)} = 1$), the first component is given by:

$$m_1^{(1)} = \frac{-c_{12}}{c_{11} - \lambda_1'}. \tag{7}$$

The plunge of this eigenvector (angle between $\mathbf{m}^{(1)}$ and the x_1-axis measured between 0 and 180°) is given by:

$$\phi = \cos^{-1}\frac{m_1^{(1)}}{|\mathbf{m}^{(1)}|} \tag{8}$$

where $|\mathbf{m}^{(1)}| = \sqrt{m_1^{(1)2} + m_2^{(1)2}}$ is the modulus of eigenvector $\mathbf{m}^{(1)}$.

2.2. Basic material deformation gradients involved in the strain pattern superposition

In order to calculate the deformation gradients $\mathbf{F}$ and $\mathbf{F}'$ in Eqs. (1) and (2) and the principal direction $\mathbf{m}^{(1)}$ in each case (Eq. (8)), factors $\mathbf{F}_{\mathrm{Sh}}$, $\mathbf{F}_{\mathrm{S}}$, $\mathbf{F}_{\mathrm{T}}$ and $\mathbf{F}_{\mathrm{F}}$ must first be obtained.

Pure (or irrotational) deformation ($\mathbf{F}_{\mathrm{P}}$). It represents a homogeneous strain whose material deformation gradient, referred to the principal directions, is:

$$\tilde{\mathbf{F}}_{\mathrm{P}} = \begin{bmatrix} \sqrt{\lambda_1^{\mathrm{P}}} & 0 \\ 0 & \sqrt{\lambda_2^{\mathrm{P}}} \end{bmatrix}. \tag{9}$$

If ϕ is the angle between the $\sqrt{\lambda_1^{\mathrm{P}}}$ principal direction and the positive side of the 1-axis (Fig. 1), the transformation matrix $\mathbf{A}$ to refer $\mathbf{F}_{\mathrm{P}}$ to the general coordinate system is:

$$\mathbf{A} = \begin{bmatrix} \cos\phi & -\sin\phi \\ \sin\phi & \cos\phi \end{bmatrix}. \tag{10}$$

Referred to this system, $\mathbf{F}_{\mathrm{P}}$ becomes:

$$\mathbf{F}_{\mathrm{P}} = \mathbf{A}\tilde{\mathbf{F}}_{\mathrm{P}}\mathbf{A}^{\mathrm{T}} = \left[F_{ij}^{\mathrm{P}}\right], \tag{11}$$

where $F_{12}^{\mathrm{P}} = F_{21}^{\mathrm{P}}$. Although ϕ can have any value between 0 and 180°, in most cases we shall consider $\phi = 90°$; then, the transformation matrix (10) becomes

$$\mathbf{A} = \begin{bmatrix} 0 & -1 \\ 1 & 0 \end{bmatrix}. \tag{12}$$

In this case, according to Eq. (11), the material deformation gradient of the pure deformation referred to the general coordinate system is:

$$\mathbf{F}_{\mathrm{P}} = \mathbf{A}\tilde{\mathbf{F}}_{\mathrm{P}}\mathbf{A}^{\mathrm{T}} = \begin{bmatrix} \sqrt{\lambda_2^{\mathrm{P}}} & 0 \\ 0 & \sqrt{\lambda_1^{\mathrm{P}}} \end{bmatrix}. \tag{13}$$

According to the ϕ-value and the timing of the pure deformation in relation to the folding, three types of pure deformation can be considered:

1. Layer shortening ($\mathbf{F}_{\mathrm{P}} \equiv \mathbf{F}_{\mathrm{Sh}}$); it occurs in the early stages of folding and has $\phi = 90°$.
2. Fold flattening ($\mathbf{F}_{\mathrm{P}} \equiv \mathbf{F}_{\mathrm{F}}$); it occurs in the late stages of folding and has $\phi = 90°$.
3. Compaction ($\mathbf{F}_{\mathrm{P}} \equiv \mathbf{F}_{\mathrm{C}}$); it involves $\phi = 0°$.

Simple shear parallel to the layer boundaries (flexural-flow). In this case, the deformation at a point of the folded layer profile can be considered a superposition of simple shear parallel to the layer boundaries $\tilde{\mathbf{F}}_{\mathrm{S}}$ and layer rotation $\mathbf{R}$. The shear amount equals the layer dip measured in radians (Ramsay, 1967, p. 393; Ghosh, 1996), that is:

$$\gamma \approx \theta_{\mathrm{S}}. \tag{14}$$

where $\theta_{\mathrm{S}} = \theta$ is the layer dip after the flexural-flow.

The material deformation gradient for the simple shear is:

$$\tilde{\mathbf{F}}_{\mathrm{S}} = \begin{bmatrix} 1 & \gamma \\ 0 & 1 \end{bmatrix} \tag{15}$$

and the rotation involved in flexural-flow is given by:

$$\mathbf{R} = \begin{bmatrix} \cos\gamma & -\sin\gamma \\ \sin\gamma & \cos\gamma \end{bmatrix}. \tag{16}$$

The result of the superposition of simple shear and rotation is:

$$\mathbf{F}_{\mathrm{S}} = \mathbf{R}\tilde{\mathbf{F}}_{\mathrm{S}}. \tag{17}$$

Tangential longitudinal strain. For this mechanism, Bobillo-Ares et al. (2000) have shown that the material deformation gradient in the reference frame defined by the vector ($\mathbf{t}$), tangent to the neutral line, and the normal vector ($\mathbf{n}$), pointing in the opposite direction to the curvature centre

(Fig. 1), is:

$$\tilde{\mathbf{F}}_T = \begin{bmatrix} 1+\kappa h & 0 \\ -\dfrac{h^2\kappa'}{2(1+\kappa h)} & \dfrac{1}{1+\kappa h} \end{bmatrix} = \begin{bmatrix} \tilde{F}_{11} & 0 \\ \tilde{F}_{21} & \tilde{F}_{22} \end{bmatrix}, \quad (18)$$

where κ is the curvature of the neutral line [characterised by a function $f(x_1)$], κ' is the derivative of the curvature with relation to the arc length of the neutral line, and h is the ordinate of the point considered within the folded layer. Since no area change is assumed, $\tilde{F}_{22} = 1/\tilde{F}_{11}$. h of a point is a function of the coordinates (X, Y) of the corresponding undeformed point and, according to Bobillo-Ares et al. (2000), it is given by:

$$h(X,Y) = \frac{\sqrt{1+2\kappa(X)Y}-1}{\kappa(X)} \quad (19)$$

where $Y > 0$ below the original neutral line and $Y < 0$ above the original neutral line. Y is the variable that will be used below to obtain the ϕ vs. θ and R vs. θ curves.

To refer $\tilde{\mathbf{F}}_T$ to the reference frame defined by base vectors $\mathbf{e}_1$ and $\mathbf{e}_2$, the latter must be related with the base vectors $\mathbf{t}$ and $\mathbf{n}$ (Fig. 1). From the intrinsic theory of curves (Struik, 1988, p. 13), we have:

$$\left.\begin{aligned} \mathbf{t} &= \beta[\mathbf{e}_1 + f'(x_1)\mathbf{e}_2] = \frac{\mathbf{e}_1 + f'(x_1)\mathbf{e}_2}{\sqrt{1+[f'(x_1)]^2}} \\ \mathbf{n} &= \beta \mathrm{sign}[f''(x_1)][f'(x_1)\mathbf{e}_1 - \mathbf{e}_2] \end{aligned}\right\}, \quad (20)$$

where

$$\beta = \frac{1}{\sqrt{1+[f'(x_1)]^2}}.$$

The columns of matrix (18) are the image components of vectors $\mathbf{e}_1$ and $\mathbf{e}_2$ in the base $(\mathbf{t}, \mathbf{n})$, that is:

$$\left.\begin{aligned} \mathbf{F}(\mathbf{e}_1) &= \tilde{F}_{11}\mathbf{t} + \tilde{F}_{21}\mathbf{n} \\ \mathbf{F}(\mathbf{e}_2) &= \tilde{F}_{22}\mathbf{n} \end{aligned}\right\}. \quad (21)$$

Introducing the expressions for $\mathbf{t}$ and $\mathbf{n}$ given by Eq. (20) in Eq. (21) and rearranging, we have:

$$\left.\begin{aligned} \mathbf{F}(\mathbf{e}_1) &= \{\tilde{F}_{11}\beta + \beta f'(x_1)\tilde{F}_{21}\mathrm{sign}[f''(x_1)]\}\mathbf{e}_1 + \{\beta\tilde{F}_{11}f'(x_1) - \beta\tilde{F}_{21}\mathrm{sign}[f''(x_1)]\}\mathbf{e}_2 \\ \mathbf{F}(\mathbf{e}_2) &= \beta f'(x_1)\tilde{F}_{22}\mathrm{sign}[f''(x_1)]\mathbf{e}_1 - \beta\tilde{F}_{22}\mathrm{sign}[f''(x_1)]\mathbf{e}_2 \end{aligned}\right\}, \quad (22)$$

and the material deformation gradient referred to the base $\mathbf{e}_1$ and $\mathbf{e}_2$ is:

$$\mathbf{F}_T = \begin{bmatrix} \tilde{F}_{11}\beta + \tilde{F}_{21}\beta f'(x_1)\mathrm{sign}[f''(x_1)] & \tilde{F}_{22}\beta f'(x_1)\mathrm{sign}[f''(x_1)] \\ \tilde{F}_{11}\beta f'(x_1) - \tilde{F}_{21}\beta\mathrm{sign}[f''(x_1)] & -\tilde{F}_{22}\beta\mathrm{sign}[f''(x_1)] \end{bmatrix} = \begin{bmatrix} F_{ij} \end{bmatrix}. \quad (23)$$

The layer dip θ at a specific point P in the initial configuration of a layer boundary can be determined taking into account that a small vector $\mathrm{d}\mathbf{X}$ at this point is deformed to vector $\mathrm{d}\mathbf{x}$ of the final configuration according to:

$$\mathrm{d}\mathbf{x} = \mathbf{F}_T\mathrm{d}\mathbf{X} \quad (24)$$

For instance, the vector $(\mathrm{d}X_1, 0)$ is transformed to the vector $(F_{11}\mathrm{d}X_1, F_{21}\mathrm{d}X_1)$, and the total rotation of the layer trace due to deformation is the final dip, which is given by:

$$\theta = \tan^{-1}\frac{F_{21}}{F_{11}}. \quad (25)$$

To analyse the strain in a fold developed by tangential longitudinal strain, it is necessary to choose a form for the function $f(x_1)$ that describes the neutral line (or the guideline when this mechanism is combined with others). The fourth-degree polynomial functions:

$$\varphi_u(x_1) = x_1^3(2-x_1) + ux_1^2\left(3 - 5x_1 + 2x_1^2\right), \quad (26)$$

for u values between 0 and 2/3 have no infinite curvature in $0 \le x_1 \le 1$ (essential condition to allow working with tangential longitudinal strain) and have an inflection point at $x_1 = 1$ (the other is outside the interval [0, 1]). To work with folds with width x_0 and amplitude y_0, we will describe the GL using a function of the type:

$$f(x_1) = y_0\left[\varphi_u\left(\frac{x_1}{x_0}\right)\right]^r; \qquad r \ge 1; \qquad 0 \le x_1 \le x_0. \quad (27)$$

Therefore, the GL is characterised by four parameters (x_0, y_0, u, r). Eq. (27) adequately describes a geometry range from forms slightly sharper than the sinusoidal shape to the box shape, including the most common fold shapes produced by the kinematical mechanisms involved in this study.

Strain patterns due to tangential longitudinal strain have been described by Bobillo-Ares et al. (2000) for folds with a sinusoidal or parabolic neutral line.

2.3. Particular cases of successive deformation superposition in fold development

The following cases of successive superposition will be analysed here: (a) layer shortening plus flexural-flow; (b) layer shortening plus tangential longitudinal strain; (c) flexural-flow plus flattening; (d) tangential longitudinal strain plus flattening; (e) layer shortening plus flexural-flow plus flattening; and (f) layer shortening plus tangential longitudinal strain plus flattening.

The resultant gradient $\mathbf{F}$ or $\mathbf{F}'$ can be obtained introducing the expressions for $\mathbf{F}_{Sh}$ (Eq. (13)), $\mathbf{F}_S$ (Eq. (17)), $\mathbf{F}_T$ (Eq. (23)) and/or $\mathbf{F}_F$ (Eq. (13)) in Eqs. (1) or (2), and substituting the gradients that are not active in the superposition by the unit matrix. The principal values and

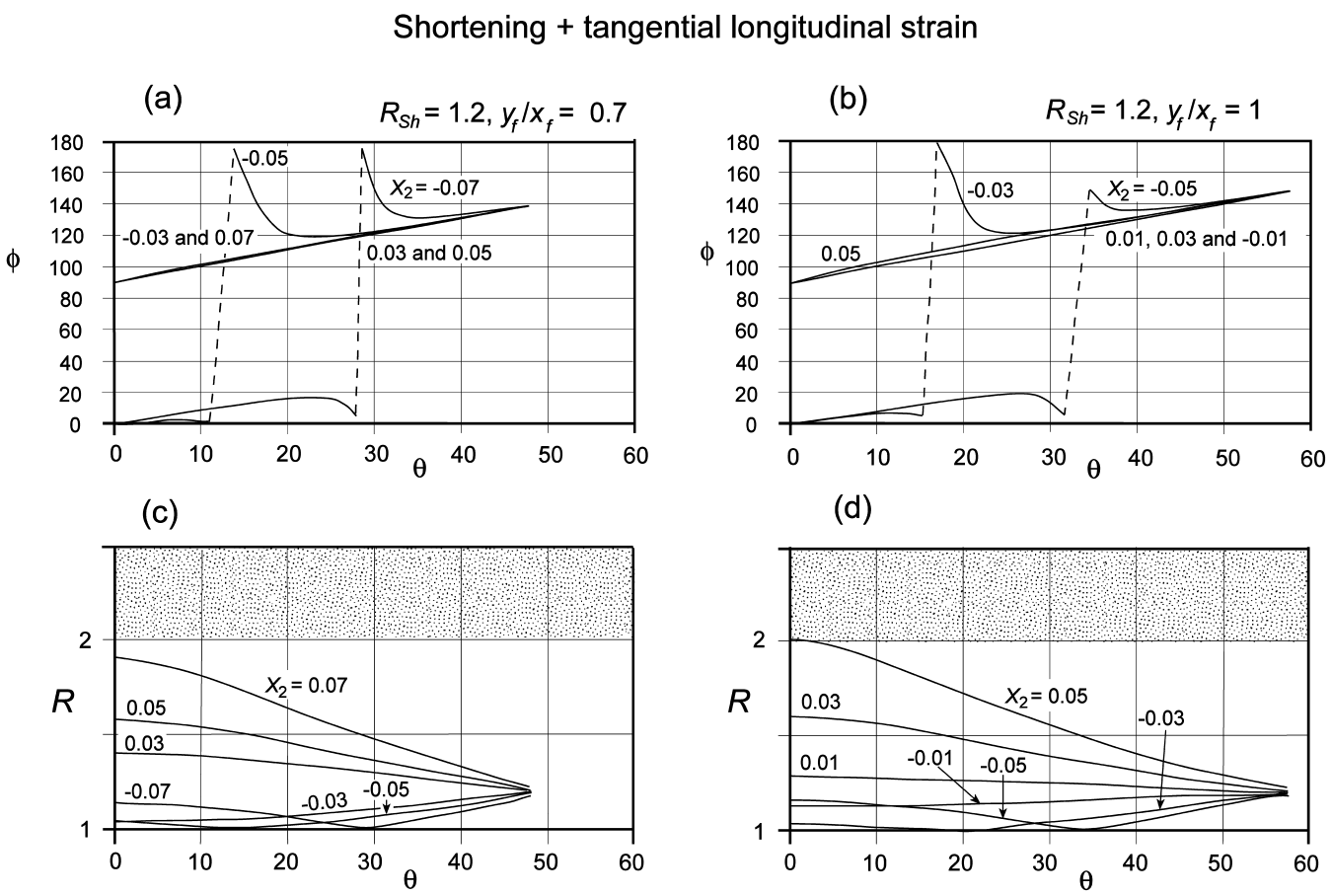

Fig. 2. $\phi-\theta$ (a and b) and $R-\theta$ (c and d) curves for folds developed by layer shortening plus tangential longitudinal strain with shortening of $R_{Sh} = 1.2$. The parameters defining the guideline are $u = 0.42$ and $r = 1$, which give a good fit of the sinusoidal shape. y_f/x_f is the aspect ratio of the fold, that is, the ratio between the maximum values of y and x of the folded guideline. Numbers on the curves indicate the ordinate Y of a layer boundary in the original configuration ($Y > 0$ for the inner arc and $Y < 0$ for the outer arc); low values of Y are necessary because the layer shortening increases the layer thickness to the extent that high $|Y|$ values make tangential longitudinal strain impossible, since area conservation is not possible. The field with $R \geq 2$ in the $R-\theta$ diagram appears ornamented.

directions of the finite strain tensor can be calculated from Eqs. (6) and (8).

Layer shortening plus flexural-flow. Making $\mathbf{F}_F = \mathbf{F}_T = \mathbf{I}$ ($\mathbf{I}$ is the unit matrix) in Eq. (1), the material deformation gradient becomes:

$$\mathbf{F} = \mathbf{F}_S\mathbf{F}_{Sh}. \tag{28}$$

This case has already been analysed by Ramsay and Huber (1987, p. 470, Fig. 21.34). According to these authors, curves ϕ vs. θ (θ' vs. $+\delta$ in Ramsay and Huber (1987)) for different values of the ratio between the shortening strain ellipse axes ($R_{Sh} = \sqrt{\lambda_1^{Sh}/\lambda_2^{Sh}}$) exhibit a minimum that tends to disappear as R_{Sh} increases. On the other hand ($R = \sqrt{\lambda_1/\lambda_2}$) vs. θ plots for several values of R_{Sh} give increasing curves, and for any value of θ, R increases with increasing R_{Sh}.

Layer shortening plus tangential longitudinal strain. Making $\mathbf{F}_F = \mathbf{F}_S = \mathbf{I}$ in Eq. (1), the material deformation gradient resulting from the superposition is given by:

$$\mathbf{F} = \mathbf{F}_T\mathbf{F}_{Sh}. \tag{29}$$

Fig. 2 shows several ϕ vs. θ and R vs. θ curves for this strain pattern combination. In the outer arc, a discontinuity is common in the ϕ vs. θ curves, so that the $\mathbf{m}^{(1)}$ directions jump from a near concentric distribution to a convergent one. This jump reflects the exchange in the orientations of the maximum and minimum strain axes where the axial ratio $R = 1$. Both the layer dip where the discontinuity appears and the area of the zone with tangential stretching increase with the fold amplitude, that is, with the progress of folding (Fig. 2a and b). This result is similar to that obtained experimentally by Gairola (1978, Fig. 9) by folding a plasticene layer in a putty matrix. The strain pattern in this case has been shown graphically by Twiss and Moores (1992) (Fig. 3). Close to the discontinuity, the curves show a minimum and a maximum that are probably due to the dominance of rotational components of the tangential longitudinal strain in locations with small values of the strain ellipse ellipticity (Bobillo-Ares et al., 2000). With higher values of layer shortening than those shown in Fig. 2, it is possible to verify that the $\mathbf{m}^{(1)}$ directions distribution

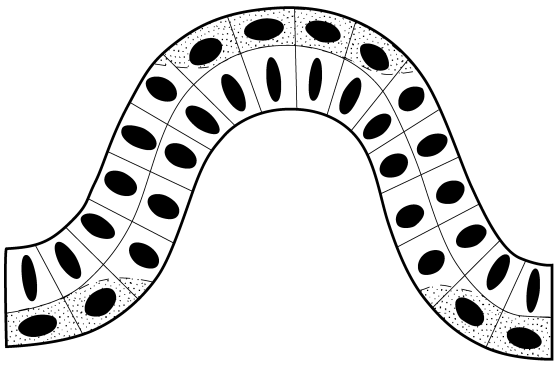

Fig. 3. Strain pattern in a folded layer by layer shortening plus tangential longitudinal strain, showing tangential stretching zones restricted to the outer arc of the hinge zone (shaded areas). The inner boundary of the shaded areas is the finite neutral line. After Twiss and Moores (1992).

becomes a convergent radial pattern both in the inner and the outer arcs.

The curves of R vs. θ show different patterns in the inner and outer arcs (Fig. 2c and d). In the inner arcs, R increases with the original distance from the neutral line and towards the hinge point. It can be checked, by constructing curves with different values of R_{Sh}, that the field with $R \geq 2$ enlarges with an increase in layer shortening. In the outer arc, the curves in Fig. 2c and d exhibit a smooth minimum, which represents the transition from the field with tangential stretching to the field with tangential shortening. For higher layer shortening than that considered in Fig. 2, the curves are always slightly increasing (minimum strain in the hinge point) in the outer arc, and $R \geq 2$ appears only when $R_{Sh} > 2$.

Flattened flexural-flow folds. This case corresponds to

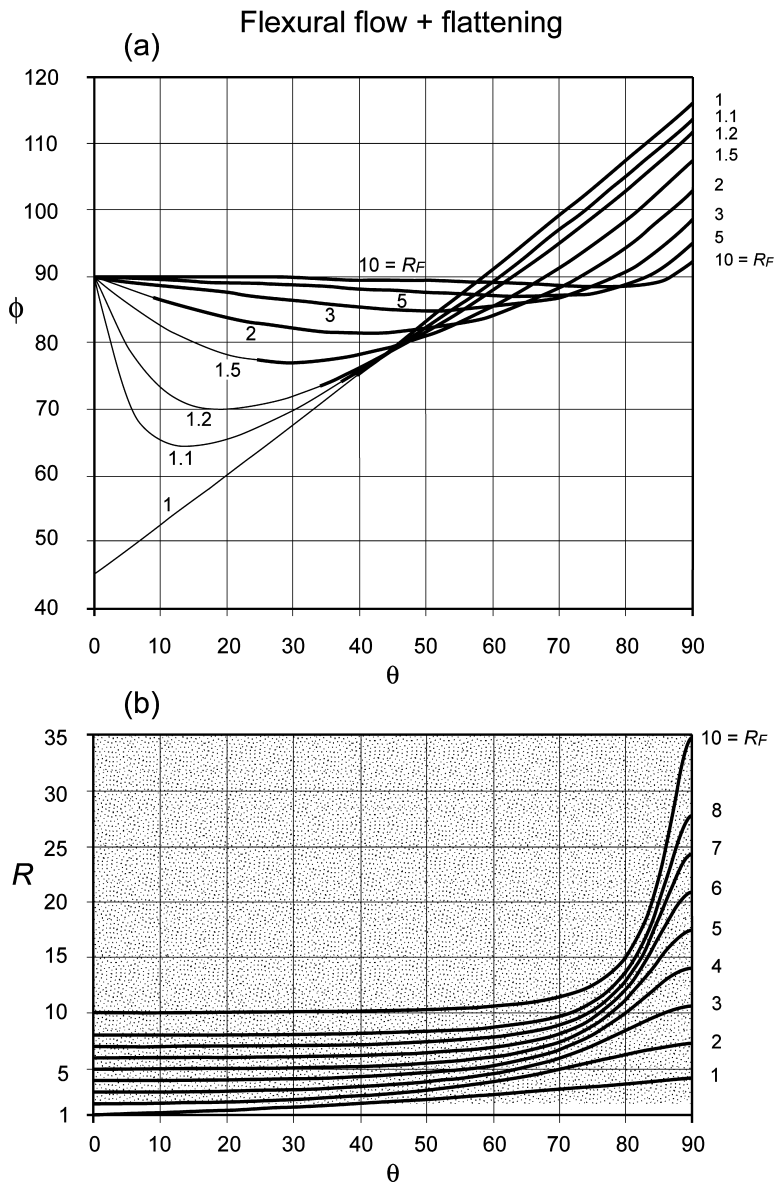

Fig. 4. $\phi-\theta$ (a) and $R-\theta$ (b) curves for folds developed by flexural-flow plus flattening with different amounts of flattening (R_F indicated by numbers on the curves). The portions of the $\phi-\theta$ curves corresponding to $R \geq 2$ are drawn with a thick line and the field with $R \geq 2$ in the $R-\theta$ diagram appears ornamented.

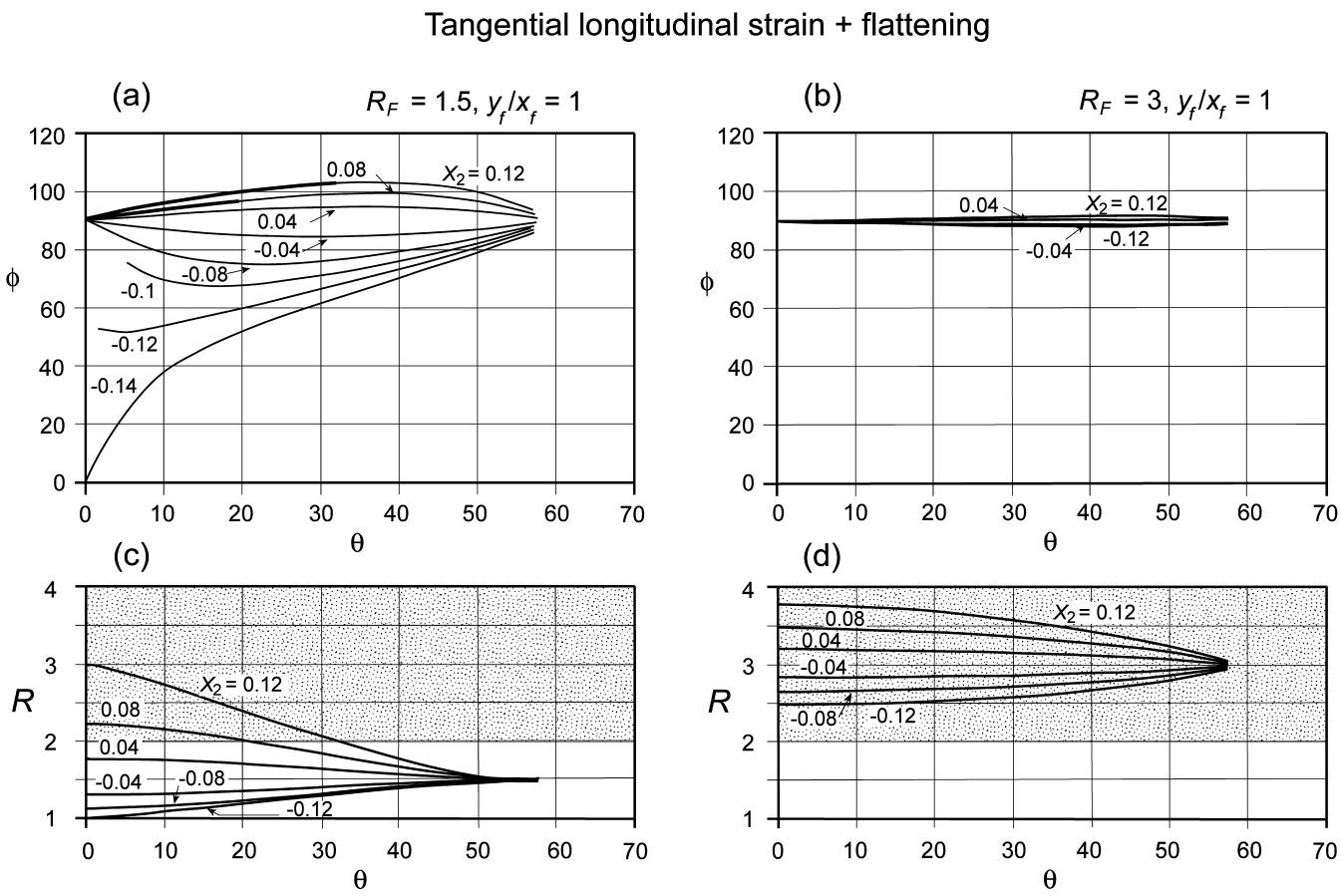

Fig. 5. $\phi-\theta$ (a and b) and $R-\theta$ (c and d) curves for folds developed by tangential longitudinal strain plus flattening with two different amounts of flattening (R_F). The parameters defining the guideline are $u = 0.42$ and $r = 1$. Numbers on the curves indicate the ordinate Y of a layer boundary in the original configuration. y_f/x_f is the aspect ratio of the fold. The portions of the $\phi-\theta$ curves corresponding to fold areas with $R \geq 2$ are drawn with a thick line and the field with $R \geq 2$ in the $R-\theta$ diagram appears ornamented.

the flattened parallel folds analysed by Ramsay (1962, 1967, pp. 411–415). The material deformation gradient for the superposition is

$$\mathbf{F} = \mathbf{F}_F\mathbf{F}_S. \tag{30}$$

In this case, the layer rotation (θ_S) involved in the flexural-flow does not equal the total layer rotation (θ) after the flattening, since the flattening produces an additional rotation of the layer. The total rotation of the layer as a result of the superposition of flexural-flow and flattening can be obtained using Eq. (25).

A set of curves of ϕ vs. θ for several amounts of flattening ($R_F = \sqrt{\lambda_1^F/\lambda_2^F}$) is presented in Fig. 4a. Each curve is characterised by a minimum that decreases in amplitude and moves towards the right for higher values of R_F. The pattern of the eigenvector $\mathbf{m}^{(1)}$ is a divergent fan for low or middle layer dips and a convergent fan for high layer dips, but as R_F increases, the $\mathbf{m}^{(1)}$ directions approach an axial plane pattern.

A set of curves of R vs. θ for several values of R_F is given in Fig. 4b. They are increasing curves, with the main step of R concentrated where large dips occur. In this part of the graph, R reaches greater values than in previous cases.

Tangential longitudinal strain plus flattening. The transformation equations are given in this case by:

$$\mathbf{F} = \mathbf{F}_F\mathbf{F}_T. \tag{31}$$

As in the previous case, the final dip θ of the folded layer results from rotation associated with tangential longitudinal strain plus rotation associated with flattening. The method to obtain θ from the material deformation gradient is the same as above.

The ϕ vs. θ curves for two amounts of flattening (R_F) (Fig. 5a and b) show that in the outer arc the concentric character of the $\mathbf{m}^{(1)}$ directions, typical of tangential longitudinal strain, becomes a divergent distribution and finally a nearly axial plane pattern as the flattening increases. In the inner arc, the $\mathbf{m}^{(1)}$ direction is normal to the layer boundary in the hinge and it exhibits a convergent distribution with a maximum ϕ value for middle dips. For high flattening, the distribution approaches an axial plane pattern.

The R vs. θ curves (Fig. 5c and d) show that, in the inner arc, the field with $R \geq 2$ enlarges with the increase in flattening until it affects the whole arc. In the outer arc, the strain is much lower than in the inner arc. The area with

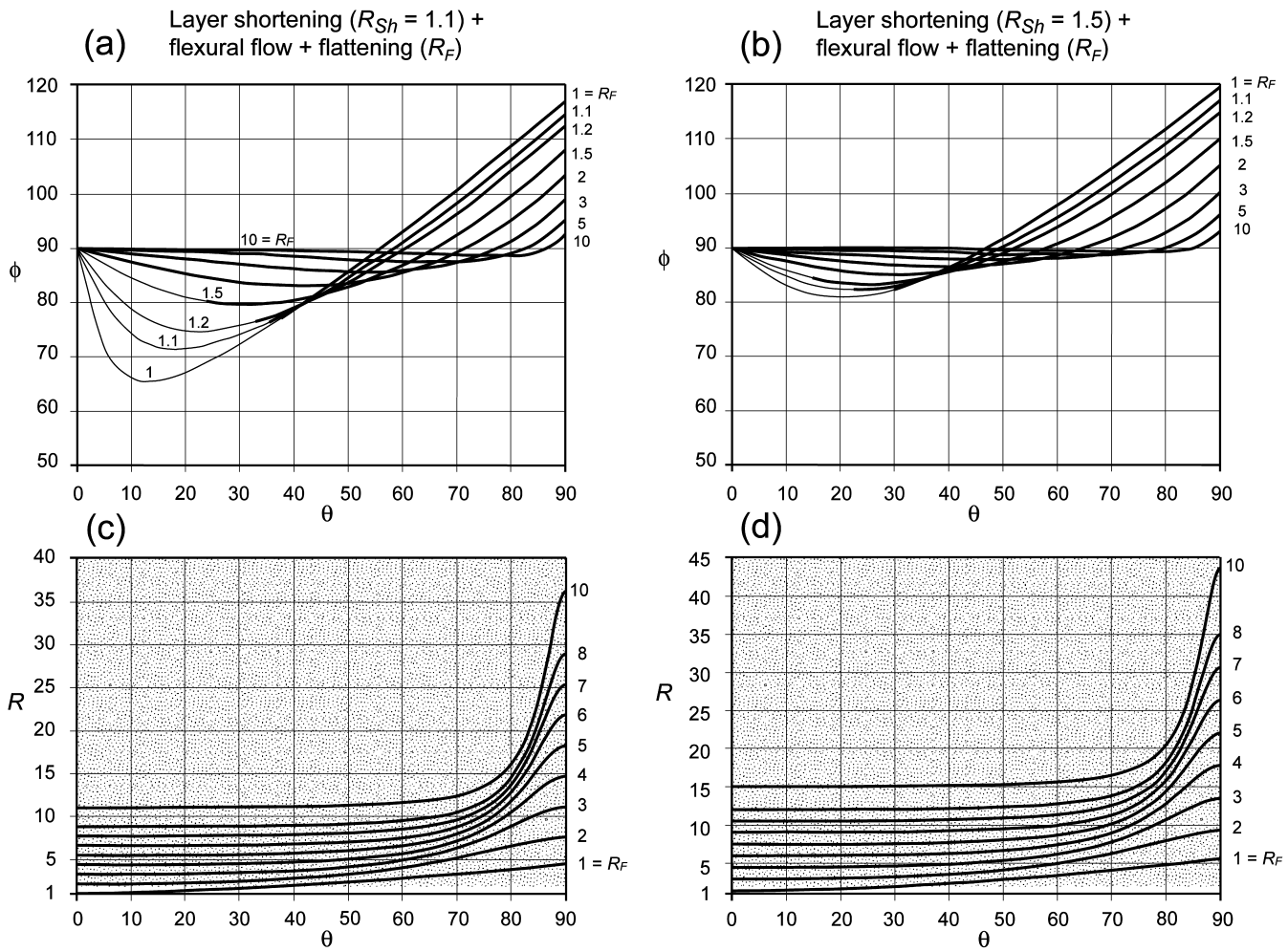

Fig. 6. $\phi-\theta$ (a and b) and $R-\theta$ (c and d) curves for folds developed by layer shortening plus flexural-flow plus flattening with different amounts of shortening (R_{Sh}) and flattening (R_F indicated by numbers on the curves). The portions of the $\phi-\theta$ curves corresponding to fold areas with $R \geq 2$ are drawn with a thick line and the field with $R \geq 2$ in the $R-\theta$ diagram appears ornamented.

$R \geq 2$ can only affect the entire outer arc when there are very high amounts of flattening, penetrating from the limb towards the hinge and outwards from the neutral line, inverse to the pattern in the inner arc.

Layer shortening plus flexural-flow plus flattening. In this case, the material deformation gradient of the superposition $\mathbf{F}$ is given by Eqs. (1) or (2), with $\mathbf{F}_T = \mathbf{I}$, and $\mathbf{F}_{Sh}$, $\mathbf{F}_S$ and $\mathbf{F}_F$ other than the unit. Many different cases can be considered depending on the amount of shortening (R_{Sh}) and flattening (R_F), and some examples are presented in Fig. 6. Fig. 6a and b shows ϕ vs. θ curves for R_{Sh} values of 1.1 and 1.5, and several R_F values from 1 to 10. The pattern of $\mathbf{m}^{(1)}$ directions is not very different from that found in flattened flexural-flow folds (compare Figs. 4a and 6a), and a tendency towards an axial plane pattern is observed as the layer shortening and/or the flattening increase. R vs. θ curves for R_{Sh} values of 1.1 and 1.5 are shown in Fig. 6c and d, respectively; they are also comparable with those for flattened flexural-flow folds (Figs. 4b and 6b), with the increase in layer shortening giving rise to an increase in the R values.

Layer shortening plus tangential longitudinal strain plus flattening. In this case, the material deformation gradient of the superposition $\mathbf{F}'$ is given by Eqs. (1) or (2) with $\mathbf{F}_S = \mathbf{I}$, and $\mathbf{F}_{Sh}$, $\mathbf{F}_T$ and $\mathbf{F}_F$ other than the unit. ϕ vs. θ curves indicate that an increase in both the shortening and flattening components enhances the homogeneity of the $\mathbf{m}^{(1)}$ direction distribution in a simple convergent pattern (Fig. 7a and b). In the R vs. θ curves, an increase in layer shortening and flattening produces an increase in the R value (Fig. 7c and d). Nevertheless, high values of one or both of these components are necessary to reach $R \geq 2$ throughout the folded layer.

3. Generalised model of strain pattern superposition in symmetric folds

Until now, we have used a simple and accurate method to analyse the successive superposition of strain patterns in folds. This method has yielded $\phi-\theta$ and $R-\theta$ curves that can be used as standards in the study of natural folds.

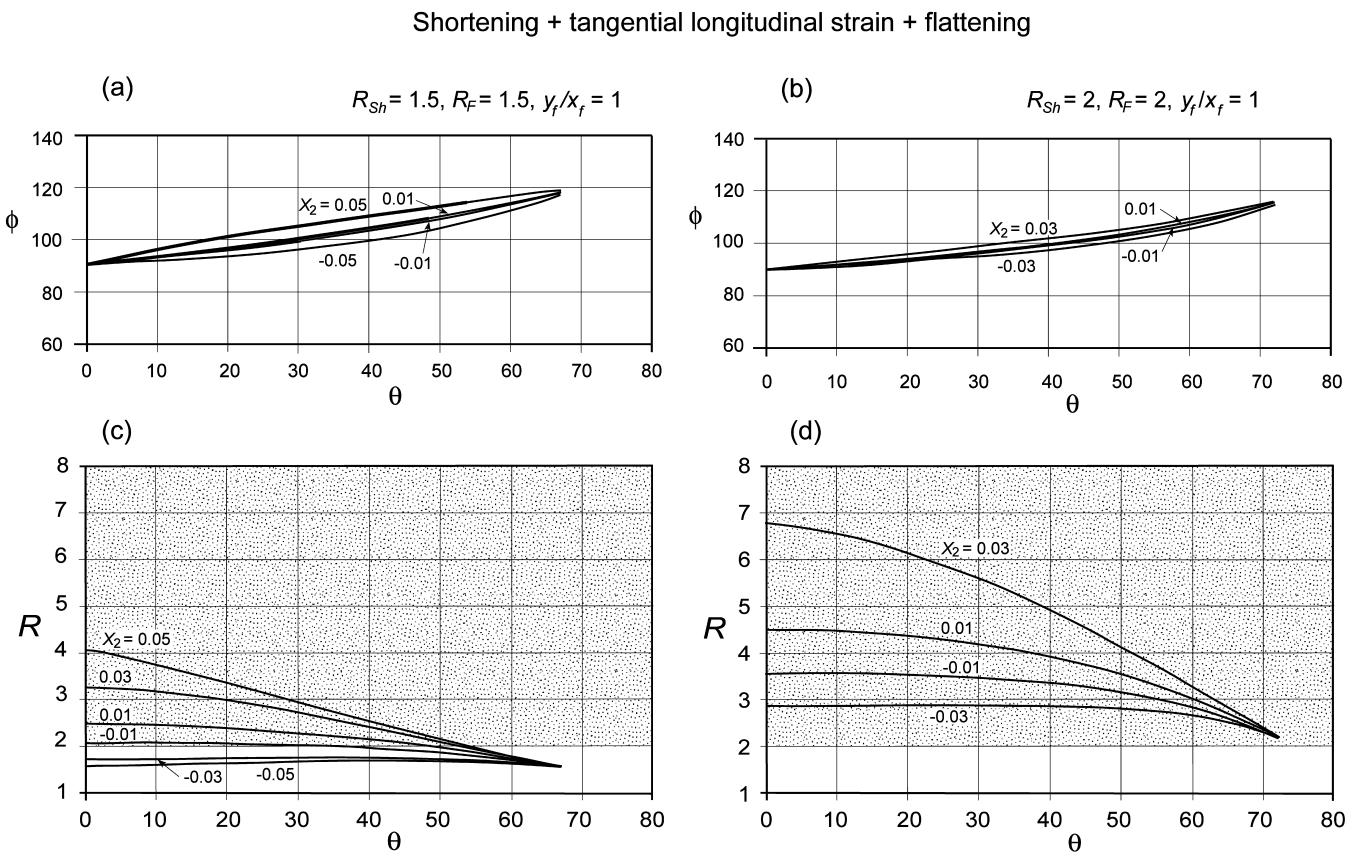

Fig. 7. $\phi-\theta$ (a and b) and $R-\theta$ (c and d) curves for folds developed by layer shortening plus tangential longitudinal strain plus flattening with different amounts of shortening (R_{Sh}) and flattening (R_F). The parameters defining the guideline are $u = 0.42$ and $r = 1$. Numbers on the curves indicate the Y ordinate of a layer boundary in the original configuration; low Y values are necessary because the layer shortening increases the layer thickness to the extent that high $|Y|$ values make the tangential longitudinal strain impossible, since area conservation is impossible. y_f/x_f is the final aspect ratio of the fold. The portions of the $\phi-\theta$ curves corresponding to fold areas with $R \geq 2$ are drawn with thick lines and the field with $R \geq 2$ in the $R-\theta$ diagram appears ornamented.

Nevertheless, it is reasonable to assume that the strain pattern superposition in natural folds is more complicated than the models considered above, because it may involve a simultaneity of mechanisms. If we try to apply the above method to these cases, many problems arise, since the mathematical treatment becomes very complicated. On the other hand, since the strain pattern superposition is not a commutative process, simultaneity cannot be simulated by simple superposition of successive strain patterns, but must be treated as a superposition of small folding steps of each of the strain patterns involved. In this part of the paper we study the superposition of many elements of strain patterns to produce folds and attempt to construct a mathematical model of more general validity.

The analysis is facilitated by the use of the guideline (GL). The following properties are assumed for this line:

- In the initial configuration, the GL is positioned midway between the layer boundaries. In this configuration, the layer and the GL are usually considered to be horizontal.
- In tangential longitudinal strain, the GL is always assumed to be a neutral line.
- In flexural-flow, the GL coincides with the shear direction, and every line parallel to the GL preserves its length during the deformation.
- In homogeneous strain (layer shortening or fold flattening), the GL is deformed according to the formulae of this strain type. Hence, the arc length, amplitude and width of the fold limb, represented by the GL, are modified; nevertheless, the curves representing the deformed and the original GL belong to the same family. It is remarkable that, when the folding involves a component of homogeneous deformation, the GL never represents a finite neutral line.
- The GL will be described by a polynomial function. Some parameters of this function (width and amplitude of the fold) will necessarily change during folding, whereas the other parameters characteristic of this function can be modified voluntarily, within their variation interval, in the different steps of the folding simulation.

A coordinate system will be introduced to describe the GL. Axis 1 is tangential to the GL at hinge point O and axis 2 is perpendicular to axis 1 at this point (Fig. 8). The unit vectors $e = (\mathbf{e}_1, \mathbf{e}_2)$ form a plane Cartesian base. If $f(x)$ is the

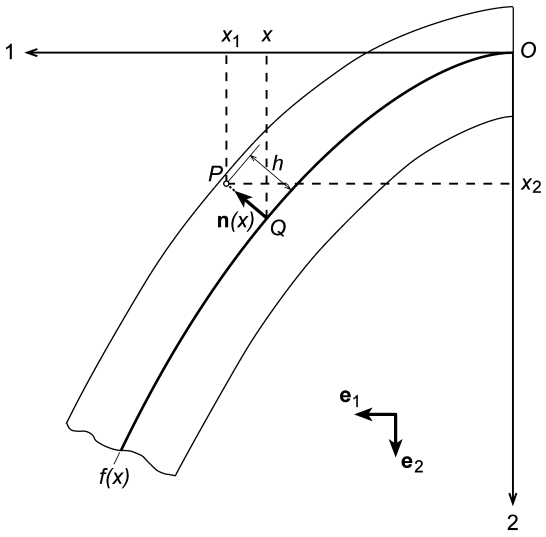

Fig. 8. Reference system ($\mathbf{e}_1$, $\mathbf{e}_2$) and coordinates used in the generalised model to define the position of a point P within the folded layer. Cartesian coordinates: (x_1, x_2); curvilinear coordinates: (x, h).

function used to represent the GL, the position vector of any point Q of the GL is:

$$\overrightarrow{OQ} = x\mathbf{e}_1 + f(x)\mathbf{e}_2. \tag{32}$$

Let us consider the line normal to the GL at Q, and the normal unit vector $\mathbf{n}(x)$ on it. Any point P belonging to the folded layer and located on the normal line has a position vector:

$$\overrightarrow{OP} = \overrightarrow{OQ} + h\mathbf{n}(x), \tag{33}$$

where h is a suitably chosen number. Therefore, any point P of the folded layer can be represented by two numbers (x, h). The first one, x, defines point Q, and the second one, h, in absolute value, indicates the distance between P and the GL ($h > 0$ for the convex part of the folded layer and $h < 0$ for the concave part); x and h will be named curvilinear coordinates of point P, and x_1 and x_2 will be named Cartesian coordinates of the same point (Fig. 8). The curvilinear coordinates (x, h) can be related to the Cartesian coordinates (x_1, x_2) by writing the vectorial Eq. (33) in the base ($\mathbf{e}_1$, $\mathbf{e}_2$). According to the mathematical theory of curves (Struik, 1988, p. 13), the normal unit vector at point $Q(x)$ is:

$$\mathbf{n}(x) = \beta\eta(m\mathbf{e}_1 - \mathbf{e}_2), \tag{34}$$

where

$$m = f'(x),$$

$$m' = f''(x),$$

$$\beta = \frac{1}{\sqrt{1+m^2}}$$

and

$$\eta = \operatorname{sign}(m').$$

Writing $\overrightarrow{OP} = x_1\mathbf{e}_1 + x_2\mathbf{e}_2$, and substituting Eqs. (32) and (34) into Eq. (33), we have the final expressions:

$$\left.\begin{aligned} x_1 &= x + h\beta\eta m \\ x_2 &= f(x) - h\beta\eta \end{aligned}\right\}. \tag{35}$$

3.1. Analysis of the strain patterns

The strain patterns considered in this model are those analysed above. However, the treatment is different here since all the strain patterns, with the exception of the first one applied, operate on a folded layer.

Tangential longitudinal strain. To obtain the image of the points of the GL, let us assume that $f(x)$ is the function that represents the guideline (GL) in the initial configuration of the corresponding folding step and that $f_t(x)$ is the corresponding function that represents the guideline (GL_t) in its final configuration, that is, after deformation by tangential longitudinal strain. Point Q on the GL has an image Q_t on the GL_t which is well determined (Fig. 9) because, as the GL is the neutral line, the arc length OQ_t on the GL_t must be equal to the arc length OQ on the GL. This condition defines a relationship between x and x_t. The length of both arcs can be obtained from the derivatives $m = f'(x)$ and $m_t = f'_t(x)$, that is:

$$\begin{aligned} \text{length of } OQ &= \int_0^x \sqrt{1+m(z)^2}\,\mathrm{d}z \\ \text{length of } OQ_t &= \int_0^{x_t} \sqrt{1+m_t(z)^2}\,\mathrm{d}z \end{aligned} \tag{36}$$

Equalising both expressions, we obtain the relationship between x and x_t, which is:

$$\int_0^x \sqrt{1+m(z)^2}\,\mathrm{d}z = \int_0^{x_t} \sqrt{1+m_t(z)^2}\,\mathrm{d}z. \tag{37}$$

To obtain the value of x_t for every x, the finite equation (37)

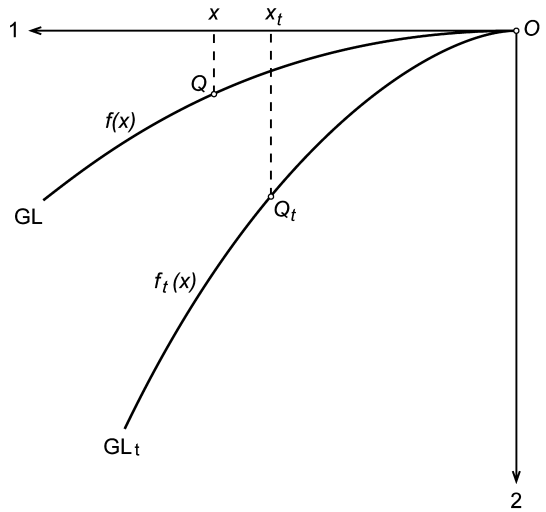

Fig. 9. Image Q_t of an initial point Q located on the guideline and folded by tangential longitudinal strain. A basic condition for this mechanism is that arc length OQ = arc length OQ_t.

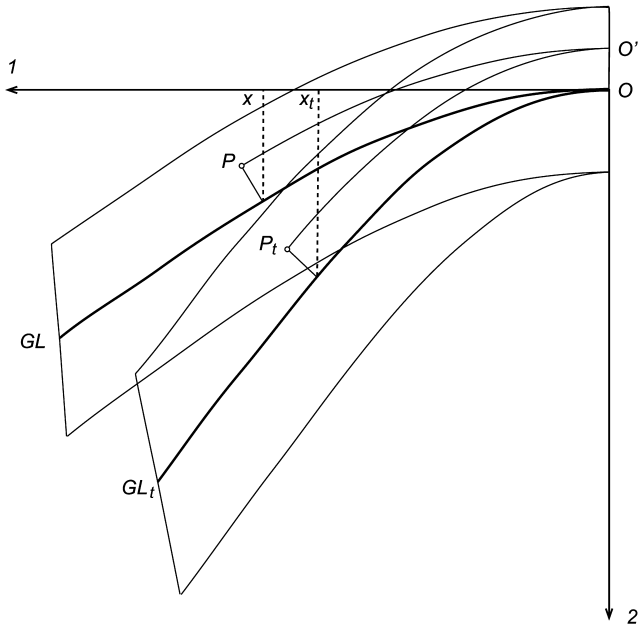

Fig. 10. Layer folded by flexural-flow. The transformation of an initial point P within the layer to an image point P_t fulfils the following basic conditions: $h = h_t$ and arc length $O'P$ = arc length $O'P_t$.

must be transformed into an ordinary differential equation. To do so, we differentiate the two members of Eq. (37) with respect to x:

$$\sqrt{1+m(x)^2} = \sqrt{1+m_t(x)^2}\,\frac{dx_t}{dx}. \tag{38}$$

The function $x_t = g(x)$ can be obtained as a solution of the ordinary differential equation:

$$\frac{dx_t}{dx} = \sqrt{\frac{1+m(x_t)^2}{1+m_t(x_t)^2}}, \tag{39}$$

with the initial condition $x_t(0) = 0$. This equation can be solved automatically using the computer environment 'MATHEMATICA'™.

To determine the image of a point that is not on the neutral line, let us consider a point P with curvilinear coordinates (x, h). The image of this point is P_t, with coordinates (x_t, h_t). In this case x_t is once again the solution of Eq. (39), and h_t can be obtained assuming area conservation. Following a method similar to that used by Bobillo-Ares et al. (2000), we obtain:

$$h_t = \frac{\sqrt{1+h\kappa_t(2+h\kappa)}-1}{\kappa_t}, \tag{40}$$

where κ is the curvature of the GL in Q and κ_t is the curvature of the GL_t in Q_t. Hence, we have the complete specification of the curvilinear coordinates of the image point P_t from those of the original point P.

Flexural-flow. In this strain pattern, the GL and every line parallel to it does not undergo length change. This condition relates points $P(x, h)$ and $P_t(x_t, h_t)$. In this mechanism, every point inside the folded layer always remains at the same distance from the corresponding GL; that is, $h_t = h$.

To relate x_t and x, we must use the condition that the arc length $O'P$ on the curve parallel through P to the GL is equal to the arc length $O'P_t$ on the curve parallel through P_t to the GL_t (Fig. 10). To represent this condition in an analytical form, we write the equations of the parallel curves by their corresponding position vector in terms of a parameter z, that is:

$$\begin{aligned}\mathbf{r}(z) &= [z\mathbf{e}_1 + f(z)\mathbf{e}_2] + \mathbf{n}(z)h\\ \mathbf{r}_t(z) &= [z\mathbf{e}_1 + f_t(z)\mathbf{e}_2] + \mathbf{n}_t(z)h\end{aligned} \tag{41}$$

where f_t is the function representing the GL_t and $\mathbf{n}_t$ is the corresponding vector. According to a well-known calculus equation:

$$\begin{aligned}\text{length of } O'P &= \int_0^x |\mathbf{r}'(z)|dz\\ \text{length of } O'P_t &= \int_0^{x_t} |\mathbf{r}'_t(z)|dz\end{aligned} \tag{42}$$

Taking into account that the length of $O'P$ = the length of $O'P_t$, we obtain the required relationship between x and x_t, that is:

$$\int_0^x |\mathbf{r}'(z)|dz = \int_0^{x_t} |\mathbf{r}'_t(z)|dz. \tag{43}$$

We can again obtain x_t in terms of x through a differential equation. To do so, we differentiate both members of Eq. (43) with respect to x, assuming that x_t is a function of x. Hence, we obtain:

$$\begin{cases}\dfrac{dx_t}{dx} = \dfrac{|\mathbf{r}'(x)|}{|\mathbf{r}'_t(x_t)|},\\ x_t(0) = 0\end{cases} \tag{44}$$

The solution of this differential equation yields x_t for every x, so that the problem of finding P_t from P in flexural-flow is solved.

Pure deformation (layer shortening and fold flattening). Let us assume a pure deformation whose principal directions coincide with those of the coordinate axes, and consider a point P of the initial folded layer with curvilinear coordinates (x, h) and Cartesian coordinates (x_1, x_2). The image of P is P_t, with curvilinear coordinates (x_t, h_t) and Cartesian coordinates (x_{1t}, x_{2t}). In Cartesian coordinates the transformation equations are:

$$\left.\begin{aligned}x_{1t} &= \sqrt{\lambda_{x_1}}x_1\\ x_{2t} &= \sqrt{\lambda_{x_2}}x_2\end{aligned}\right\} \tag{45}$$

where λ_{x_1} and λ_{x_2} are the quadratic elongations in the direction of the coordinate axes. These quadratic elongations are principal values of the strain and are usually, but not necessarily, $\lambda_{x_2} = \lambda_1$.

If the GL of the initial fold is $f(x)$ and the GL of the

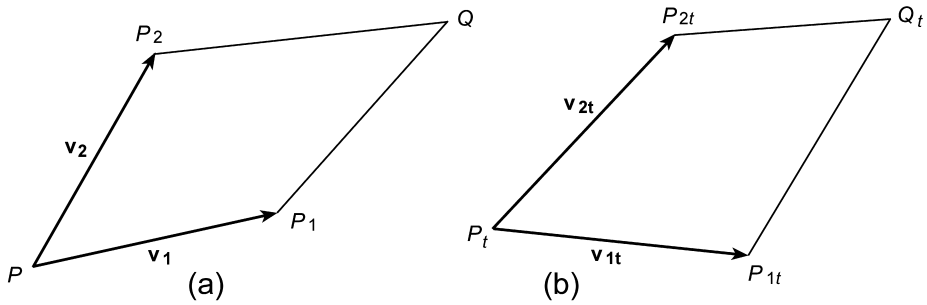

Fig. 11. Initial (a) and deformed (b) configurations corresponding to a folding step for an individual quadrilateral of the layer grid.

deformed fold is $f_t(x)$, the two are related by:

$$f_t(x) = \sqrt{\lambda_{x_2}} f\left(\frac{x}{\sqrt{\lambda_{x_1}}}\right). \tag{46}$$

The transformation equations (45), together with Eq. (35), which gives the change of coordinates, yield:

$$\left.\begin{aligned} x_1 &= x + h\beta\eta(x)m(x) \\ x_2 &= f(x) - h\beta(x)\eta(x) \end{aligned}\right\}, \tag{47}$$

$$\left.\begin{aligned} x_{1t} &= x_t + h_t\beta\eta_t(x_t)m_t(x_t) \\ x_{2t} &= f_t(x_t) - h_t\beta_t(x_t)\eta_t(x_t) \end{aligned}\right\}. \tag{48}$$

These equations allow (x_t, h_t) to be found in terms of (x, h), although, to do so, the nonlinear system (48) must be solved. This solution can be obtained automatically using the computer environment 'MATHEMATICA'™.

3.2. Characterisation of a transformation

A fold is characterised by specifying its GL, which can be done by choosing a function family of the same form as Eq. (27), that is, in this case:

$$f(x) = y_0\left[\varphi_u\left(\frac{x}{x_0}\right)\right]^r; \qquad r \geq 1, \qquad 0 \leq x \leq x_0, \tag{49}$$

with

$$\varphi_u(x) = x^3(2-x) + ux^2(3-5x+2x^2); \qquad 0 \leq u \leq 2/3. \tag{50}$$

A transformation is specified giving the parameters (x_0, y_0, u, r) of the original GL and the corresponding parameters $(x_{0t}, y_{0t}, u_t, r_t)$ of the final GL, defined by the equation:

$$f_t(x) = y_{0t}\left[\varphi_{u_t}\left(\frac{x}{x_{0t}}\right)\right]^{r_t}; \qquad r_t \geq 1, \qquad 0 \leq x \leq x_{0t}. \tag{51}$$

In addition, in order for the transformation to be perfectly defined for every point of the folded layer, the mechanism used in the transformation must be specified (tangential longitudinal strain, flexural-flow or pure deformation).

3.3. Analysis of the state of strain within the folded layer

The mathematical description of the three mechanisms involved is complicated, so that obtaining each image point requires the numerical solution of nonlinear equation systems. Unfortunately, we cannot obtain explicit equations, expressed in terms of elementary functions, which would directly give the coordinates (x_t, h_t) of an image point in terms of the coordinates (x, h) of the original point. Hence, we cannot obtain the deformation gradient by direct derivation either. We will use a non-exact method to overcome this difficulty, but the error can be made as small as we like.

We have divided the folded layer into quadrilaterals, which are small enough to assume nearly homogeneous strain within them. Afterwards, using the mathematical methods described above, we obtained the images of the vertices of the original quadrilaterals. Analysing the relation between each original quadrilateral and the corresponding deformed quadrilateral, it is possible to approximately obtain the deformation gradient at any point of the quadrilateral. The error can be made as small as we want by making the quadrilaterals sufficiently small.

Obtaining the strain tensor approximately. To numerically obtain the deformation gradient, we must search for the simplest quadratic relationship between the four original points and their corresponding images. Deriving these relationships, it is possible to obtain the deformation gradient at any point of the quadrilateral.

Let P, P_1, P_2 and Q be the four vertices of the original quadrilateral, and P_t, P_{1t}, P_{2t} and Q_t the corresponding points of the deformed quadrilateral (Fig. 11). First of all, an expression must be found for the points inside the original quadrilateral. Taking P as origin, any point T of this quadrilateral is obtained by the equation:

$$\overrightarrow{PT} = s_1\mathbf{v}_1 + s_2\mathbf{v}_2 + s_1s_2\mathbf{w} \tag{52}$$

where $\mathbf{v}_1 = \overrightarrow{PP_1}$, $\mathbf{v}_2 = \overrightarrow{PP_2}$ and $\mathbf{w}_t = \overrightarrow{PQ} - \mathbf{v}_1 - \mathbf{v}_2$. Varying s_1 and s_2 between zero and one, it is possible to obtain all the points inside and on the boundaries of the quadrilateral. Particularly, points P, P_1, P_2 and Q correspond, respectively, to the following values of (s_1, s_2): (0, 0), (1, 0), (0, 1) and (1, 1).

(a)

p1 = {1, 0, 0.42, 1}

block1 = {1, {3, 0.72, 1}}
block2 = {1, {1, 0.33, 0, 0}, {2, 0.07, 0, 0}}
block3 = {1, {3, 0.67, 1}}

	Theoretical Fold	Natural Fold
Aspect Ratio (y_f /x_f)	0.891	0.897
t_0/y_{oa}	1.48	1.54

Theoretical Bulk Shortening = 55.84%

(b)

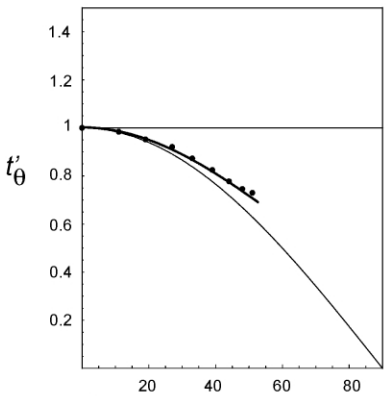

(c)

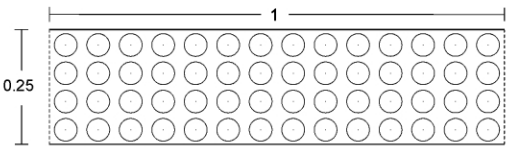

(d)

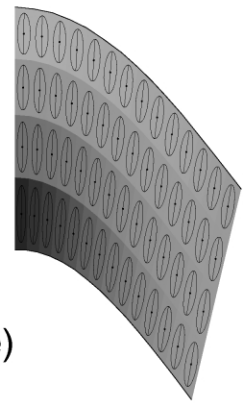

(e)

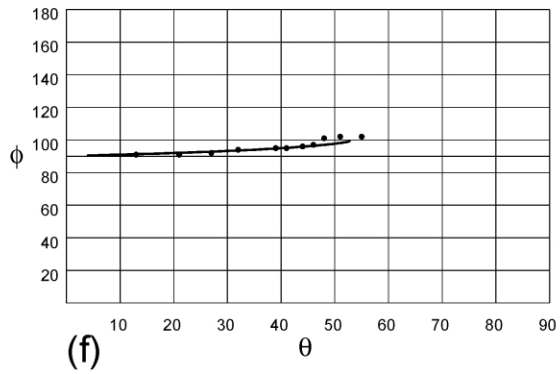

(f)

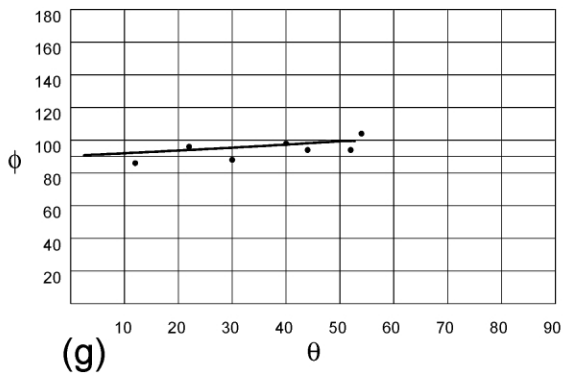

(g)

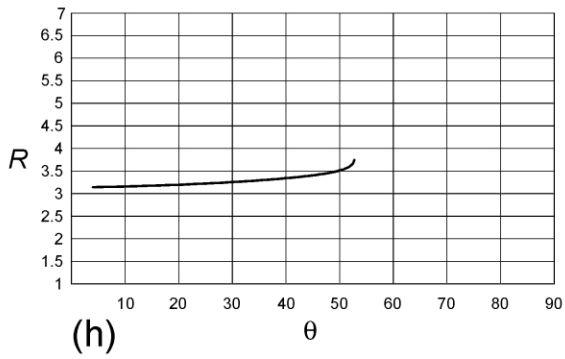

(h)

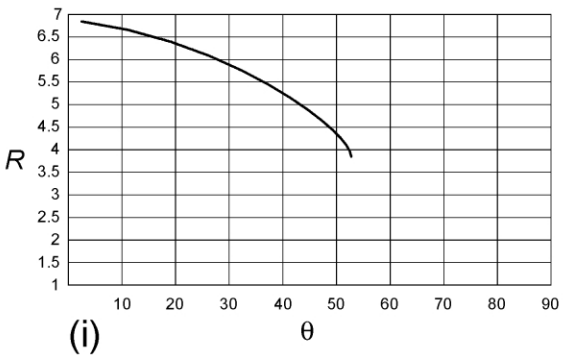

(i)

Expressions for the points of the deformed quadrilateral can be found in the same way; that is:

$$\overrightarrow{P_tT_t} = s_1\mathbf{v}_{1t} + s_2\mathbf{v}_{2t} + s_1s_2\mathbf{w}_t, \tag{53}$$

where $\mathbf{v}_{1t} = \overrightarrow{P_tP_{1t}}$, $\mathbf{v}_{2t} = \overrightarrow{P_tP_{2t}}$ and $\mathbf{w}_t = \overrightarrow{P_tQ_t} - \mathbf{v}_{1t} - \mathbf{v}_{2t}$.

Let us assume that the image of point T is approximately point T_t, with both points corresponding to the same values of s_1 and s_2. The transformation based on this supposition does not in general involve a homogeneous deformation, so that the deformation gradient depends on the point considered in the quadrilateral. At any point T of the original quadrilateral, let us consider the small vectors:

$$\left.\begin{aligned} d_1\overrightarrow{PT} &= \frac{\partial\overrightarrow{PT}}{\partial s_1}\mathrm{d}s_1 = \mathbf{u}_1\mathrm{d}s_1;\ \text{where } \mathbf{u}_1 = \mathbf{v}_1 + s_2\mathbf{w} \\ d_2\overrightarrow{PT} &= \frac{\partial\overrightarrow{PT}}{\partial s_2}\mathrm{d}s_2 = \mathbf{u}_2\mathrm{d}s_2;\ \text{where } \mathbf{u}_2 = \mathbf{v}_2 + s_1\mathbf{w} \end{aligned}\right\} \tag{54}$$

Their images are also small vectors located at T_t (s_1, s_2):

$$\left.\begin{aligned} d_1\overrightarrow{P_tT_t} &= \frac{\partial\overrightarrow{P_tT_t}}{\partial s_1}\mathrm{d}s_1 = \mathbf{u}_{1t}\mathrm{d}s_1;\ \text{where } \mathbf{u}_{1t} = \mathbf{v}_{1t} + s_2\mathbf{w}_t \\ d_2\overrightarrow{P_tT_t} &= \frac{\partial\overrightarrow{P_tT_t}}{\partial s_2}\mathrm{d}s_2 = \mathbf{u}_{2t}\mathrm{d}s_2;\ \text{where } \mathbf{u}_{2t} = \mathbf{v}_{2t} + s_1\mathbf{w}_t \end{aligned}\right\} \tag{55}$$

The material deformation gradient $\mathbf{F}$ in (s_1, s_2) is a linear operator, and hence, it is determined specifying its effect on two linearly independent vectors, that is:

$$\left.\begin{aligned} d_1\overrightarrow{P_tT_t} &= \mathbf{F}\left(d_1\overrightarrow{PT}\right) \\ d_2\overrightarrow{P_tT_t} &= \mathbf{F}\left(d_2\overrightarrow{PT}\right) \end{aligned}\right\} \tag{56}$$

Cancelling the differential coefficients ds_1 and ds_2, we obtain the finite relationships:

$$\mathbf{u}_{1t} = \mathbf{F}(\mathbf{u}_1); \qquad \mathbf{u}_{2t} = \mathbf{F}(\mathbf{u}_2). \tag{57}$$

The matrix of $\mathbf{F}$ in the bases $u = (\mathbf{u}_1, \mathbf{u}_2)$ and $u_t = (\mathbf{u}_{1t}, \mathbf{u}_{2t})$ is the unit matrix $\mathbf{I}$; hence, the matrix $\mathbf{F}_e$ is obtained in the Cartesian base $e = (\mathbf{e}_1, \mathbf{e}_2)$ through the corresponding base changes:

$$\mathbf{F}_e = \mathbf{B}^{-1}\mathbf{I}\mathbf{A} = \mathbf{B}^{-1}\mathbf{A}, \tag{58}$$

where $\mathbf{A}$ is the matrix of base change from $u = (\mathbf{u}_1, \mathbf{u}_2)$ to the Cartesian base e, and $\mathbf{B}$ is the matrix of base change from $u_t = (\mathbf{u}_{1t}, \mathbf{u}_{2t})$ to the Cartesian base e. From $\mathbf{F}_e$, Cauchy's finite strain tensor and its principal directions and values can be determined by the method described in the first part of this paper.

4. Geological application

In Section 2, curves have been obtained (Figs. 2 and 4–7) that describe the main features of folds originated by several combinations of strain patterns. These curves can be used as standards for comparison with curves obtained from natural folds. ϕ vs. θ curves can be easily obtained from cleavage patterns in natural folds. In this way, it is possible to obtain a first approach to the kinematical mechanisms involved in the formation of natural folds. This information can provide some useful keys for further analysis using the general method described in Section 3.

The theory developed in Section 3 has been used to construct a computer program that generates theoretical folds for any combination of the strain patterns considered (tangential longitudinal strain, flexural-flow and pure deformation by layer shortening or fold flattening). The environment 'MATHEMATICA'™ has been used for this purpose. All the geometrical characteristics of the theoretical folded layer produced by this method can be easily determined. The input data to run this program are:

- Data on the initial form of the folded layer. The input data set $p1$ consists of four parameters that characterise the GL: initial value of x_0 of the fold (usually the unit), initial value of y_0 (initial amplitude, usually zero), and values of u and r (they define the shape of the GL). An example of input data is shown in Fig. 12b ($p1 = \{1, 0, 0.42, 1\}$).
- Data on the grid of parallelograms that mark the strain within the folded layer: number of parallelograms along the folded layer, and number and height of the parallelograms to place above and below the GL.
- Data on the strain patterns involved in the folding. They depend on the type of strain pattern. In tangential longitudinal strain and flexural-flow (termed patterns 1 and 2, respectively), it is necessary to introduce the increment in normalised amplitude (y_0/x_0) and the increments in u and r that each mechanism must produce every time it is considered. In pure deformation (named pattern 3), every time that this mechanism is considered, it is necessary to introduce the value of λ_{x_1} (usually $\sqrt{\lambda_2}$) and the value of the area change (ratio between final area and initial area, that is, the jacobian of the material

Fig. 12. Fit of a natural fold using the general model. (a) Antiform developed in a lower Cambrian sandstone near Cudillero (Spain) whose right limb has been fitted. (b) Input data characterising the theoretical fold (p1, block1, block2, block3), and comparison of some outputs of the theoretical fold with the corresponding parameters of the natural fold (t_0/y_{0a} is the ratio between the hinge thickness and the amplitude of the outer arc). (c) Ramsay's classification of the theoretical folded layer (line) and the natural fold (dots). (d) Initial configuration of the theoretical layer. (e) Folded configuration of the theoretical layer showing the strain ellipses and shading proportional to the aspect ratio of the strain ellipses. (f) and (g) $\phi-\theta$ diagrams for the outer and inner arcs, respectively, showing the data obtained from the theoretical folded layer (line) and the natural fold (dots). (h) and (i) $R-\theta$ diagrams for the outer and inner arcs, respectively, showing the strain pattern predicted for the theoretical fold.

deformation gradient). The strain patterns are introduced in blocks. The same mechanism can be introduced repeatedly in a single block. An example is shown in Fig. 12b, in which block2 = {1, {1, 0.33, 0, 0}, {2, 0.07, 0, 0}} has three parts: the first one is a whole number (one in this case), which indicates the number of times that the strain patterns involved in the block will be executed (once in this case); the second one is a set that indicates a folding step in which pattern 1 is applied (tangential longitudinal strain) with an amplitude of 0.33, and without changes in the parameters u and r; the third one is a set that indicates a folding step in which pattern 2 (flexural-flow) is applied with an amplitude increment of 0.07, and without changes in the parameters u and r. Although only two folding steps have been included in this example, in general, more steps can be introduced in a single block. Several blocks can be included in a single program and executed sequentially.

- Data on the ornamentation of the folded layer profile. The main data of this type refer to the representation of the strain ellipse and/or their axes, and to the definition of a grey level to enhance several features of the folded layer, such as, for instance, the ellipticity variation of the strain ellipse.

The program outputs a large amount of information about the geometry and the state of strain of the folded layer, including the following data (Fig. 12):

- The ellipticity of the strain ellipse corresponding to each folding step of pure deformation introduced in the model.
- The bulk shortening associated with the folding.
- The value of the final amplitude ($y_0 = y_f$) and width of the fold ($x_0 = x_f$), as well as the ratio between these two parameters (final normalised amplitude y_f/x_f).
- The values of the u and r parameters characteristic of the final GL.
- The ratio between the thickness at the point with dip zero and the amplitude of the outer arc of the folded layer.
- The drawing of the folded layer, showing the deformed grid of parallelograms, the distribution of strain ellipses and their axes, and a variation in the grey level depending on the ellipticity of the strain ellipse.
- The $\phi-\theta$ and $R-\theta$ curves for the inner and outer arcs of the folded layer.
- Ramsay's classification of the folded layer.

Summarising, the model provides complete information about the folded layer generated theoretically for any chosen combination of strain patterns considered. This information can be used to predict geological features that can appear in folded rocks.

This method can also be used to analyse the folding mechanisms involved in the development of natural folds, since adequate information about the geometry and cleavage distribution in a natural folded layer enables its fit by modelled folds; the interpretation of the results can help to clarify many features of the development of the natural fold. In addition, the method makes the kinematical analysis of folds produced by experimental or numerical methods possible, such as the finite element method; in these cases, the analysis is facilitated by the knowledge of the initial and intermediate configurations. The information from a natural fold, or any other fold type, necessary to fit it with a theoretical fold is:

- Geometry of the folded surfaces. This analysis can be made using the classification method developed by Bastida et al. (1999), from which it is possible to obtain, for the bottom and the top of the bed, the ratio y_0/x_0 and the exponent n of the corresponding power functions. The values of y_0/x_0 and n of the GL can be approximated with the mean value of these parameters for the bottom and the top. For a theoretical approximation of a natural fold, each power function with exponent n can be approximated by a fourth-grade polynomial function with certain values for parameters u and r. To find these parameters, we define the quadratic error as:

$$E = \int_0^1 [x^n - \varphi_u(x)^r]^2 \mathrm{d}x \tag{59}$$

  The u and r values are found by minimising error E.
- The ratio between the layer thickness at the point with dip zero and the amplitude of the outer arc of the folded layer.
- The axial direction and the axial surface orientation of the fold.
- The $\phi-\theta$ curves for the inner and outer arcs of the folded layer. These curves can be determined by measuring dips of the bedding and primary cleavage at as many points of the bottom and the top of the folded layer as possible. This method assumes that the cleavage surfaces are perpendicular to the direction of maximum finite shortening. Since, in the theoretical models, the profile plane and the axial trace are vertical, the orientation of the axis and the axial surface of the natural folds must be rotated by stereographic projection methods until the axis becomes horizontal and the axial surface vertical. This rotation must also be applied to the bedding and cleavage surfaces used to obtain the $\phi-\theta$ curves.
- Ramsay's classification of the folded layer.
- If possible, the strain ratio R should be obtained at points of the layer boundaries to construct $R-\theta$ curves.

Information about the variation of the R ratio through a natural folded layer is not generally available. However, if the rest of the information above about the folded layer is available, many good fits with theoretical folds with different $R-\theta$ curves for the layer boundaries can be found in many cases. These fits present different patterns of kinematical mechanism superposition and finding the one that best describes the kinematical history of the natural fold

is difficult. Nevertheless, the superposition patterns for these fits usually have some common features that enable some conclusions to be drawn about the mechanisms involved in the folding. A better approximation to the knowledge of the strain pattern and the kinematical history of a natural folded layer requires a few complementary strain measures at least.

The general fitting method described above has been applied to many natural folds using a trial-and-error method and taking as a basis the $\phi-\theta$ curves obtained in Section 2 and standard curves obtained applying the generalised model. An example of a good fit is shown in Fig. 12. In this case, an approximately sinusoidal GL has been deduced for the natural fold and used in the theoretical model (parameters u and r equal to 0.42 and 1, respectively, in $p1$ of Fig. 12b). The initial thickness is 0.25 (Fig. 12d). The strain patterns involved in the fold steps of the model are: (I) an initial pure deformation with $\sqrt{\lambda_{x_1}} = \sqrt{\lambda_2} = 0.72$ and without area change, that is, $\sqrt{\lambda_1/\lambda_2} = 1.93$; (II) tangential longitudinal strain giving rise to an amplitude of 0.33; (III) flexural-flow giving rise to an amplitude increment of 0.07; and (IV) pure deformation with $\sqrt{\lambda_{x_1}} = \sqrt{\lambda_2} = 0.67$ and without area change, that is, $\sqrt{\lambda_1/\lambda_2} = 2.23$. By trial-and-error, 0.25 is the maximum thickness found that yields a good fit, but good fits different to that in Fig. 12 are also possible for any initial thickness >0 and ≤ 0.25. All these fits have roughly similar amounts of tangential longitudinal strain (0.25–0.4), flexural flow (0–0.15) and fold flattening (0.65–0.77); the main difference between them is in the amount of layer shortening (0.28–0.74) and consequently of bulk shortening (any value $\geq 54.6\%$ and $<100\%$ is possible). For a specific thickness, slight variations can be made in the folding steps that keep a good fit. For example, for the thickness of 0.25 considered in Fig. 12, the amount of tangential longitudinal strain can vary between 0.3 and 0.4, flexural-flow between 0 and 0.09 and total pure deformation between 0.46 and 0.51.

In the above analysis, no area change has been allowed in the model. Nevertheless, volume changes of up to 10% during deformation are probably common in deformed rocks; greater changes are probably rare (Wood, 1974; Tan et al., 1995). Good fits involving area changes of up to 10% in the pure deformation folding steps only require minor changes in the amount of the kinematical mechanisms involved in the model. The most remarkable change is produced in layer shortening, which increases as the area decreases. In the models analysed, for an area change of 10%, the bulk shortening can increase up to about 3%, depending on the initial thickness.

According to our results, the natural folds that can be fitted by the method proposed generally allow an infinite number of fits. Evidently, all these fits are not equally probable. One set of fits involves huge values of R and bulk shortening and is geologically unrealistic. The discrimination of an interval of geologically realistic fits can be made in each case from structural considerations. The availability of strain data from the folded rocks is the key for a maximum reduction of the field of possible fits. In these cases, the method is to find the fits that have curves $R-\theta$ fitting the strain measurements.

5. Discussion and conclusions

The analysis of the deformation gradients of some folding mechanisms forming symmetric folds has been used to obtain theoretical models of folds resulting from simple combinations of these mechanisms. Each strain pattern (layer shortening, tangential longitudinal strain, flexural-flow and fold flattening) is characterised by a deformation gradient, and the multiplication of selected gradients in the proper order determines the state of strain in the folded layers. This state has been described by two types of graphs: the first one represents the orientation (angle ϕ) of the major axis of the strain ellipse on the fold profile plane as a function of the dip layer θ and the second one represents the aspect ratio R of the strain ellipse as a function of θ. In this way, it is possible to obtain families of standard curves that can be used as a basis for the strain analysis of folds. Cleavage has been considered as the reference ductile structure that can appear in folds when the ratio R is large. The following conclusions can be drawn from our analysis:

- The development of cleavage is improbable in folds formed by flexural-flow. It could only be possible for dip values greater than those usually reached by beds affected by this folding mechanism.
- In sinusoidal and nearly sinusoidal folds originated by layer shortening plus tangential longitudinal strain, the presence and extension of cleavage mainly depend on the amount of layer shortening. As it increases, cleavage appears first in the inner arc of the hinge zone far from the guideline; then, it progresses towards the guideline and the fold limb; finally, it can penetrate the outer arc, from the limbs towards the hinge. In this type of folding the cleavage would be strongly convergent.
- In folds originated by layer shortening plus flexural-flow, as the shortening increases the cleavage progresses from the limbs towards the hinge. The cleavage would be divergent in an interval of lesser dips and convergent for higher dips. Nevertheless, if the shortening is high, the cleavage pattern can be a convergent fan throughout the entire fold.
- In sinusoidal and nearly sinusoidal folds generated by tangential longitudinal strain plus flattening, the pattern of increase of the R value through the fold during its development is similar to that found in folding by layer shortening plus tangential longitudinal strain. Nevertheless, the possible cleavage pattern is different since in this case it would be a convergent fan in the inner arc and a divergent fan in the outer arc; both arcs would tend to have axial plane cleavage with very large amounts of flattening.

- The cleavage pattern of the flattened flexural-flow folds or the folds originated by layer shortening plus flexural-flow is not very different from that of the folds involving layer shortening plus flexural-flow plus flattening. The strain ratio is higher in the zone near the inflection points than in other parts of the fold, and the cleavage progresses from the limbs towards the hinge zone. The cleavage pattern is dominantly divergent, although it tends to an axial plane pattern for large amounts of flattening.
- In sinusoidal and nearly sinusoidal folds originated by layer shortening plus tangential longitudinal strain plus flattening, the cleavage would appear first in the hinge zone of the inner arc and then progress through the entire structure as the shortening and flattening increased. The cleavage pattern predicted is a convergent fan, tending to an axial plane pattern with high shortening and flattening.

The strain analysis in folds using deformation gradients is limited to simple cases of folding, because the mathematical treatment to find the final deformation gradient is very complicated when tangential longitudinal strain or flexural-flow are applied to a previously folded layer. An alternative theoretical method of more general validity has been developed to avoid this complication. In this method each mechanism operates during a folding step, so that the initial configuration of the step is generally a folded form and the final configuration of the step corresponds to the same folded layer with slightly higher amplitude. The method consists in applying the properties of each mechanism to find the image point of any initial point for each step. After the superposition of a finite number of folding steps, it is possible to obtain a grid of deformed points derived from those of the original grid. The analysis of the deformed grid reveals the geometry and the strain distribution on the folded layer. Hence, this general method is a powerful tool to theoretically analyse the geometry and kinematics of folds originated by any successive or simultaneous superposition of the mechanisms involved in the modelling (layer shortening, tangential longitudinal strain, flexural-flow and fold flattening).

The results of the latter fold modelling method can be applied to the analysis of the geometry and strain patterns in natural and experimental folds. Particularly, in a natural fold, when the geometry of the folded layer and surfaces, and the dip of the bedding vs. dip of the cleavage are known, we can try to fit these data with theoretically modelled folds. Nevertheless, several constraints condition how the fits are obtained and interpreted.

The first limitation is that the general method only models symmetric folds. Another limitation is given by the possible influence in natural folds of strain patterns that have not been considered in the modelling method. Mechanisms such as neutral line migration or heterogeneous area change during folding are probable in folds formed by tangential longitudinal strain with high deformation, and neglecting them can give rise to errors. Flexural-slip is a frequent folding mechanism in multilayered systems, but is rare in individual layers and has therefore not been considered in this paper. Heterogeneous simple shear across the layers is probably infrequent in nature (González-Bonorino, 1970; Ramberg, 1963) and has not been considered here either. Another limitation of the method appears in incompetent layers adjacent to competent levels, since mechanisms not considered in our models, such as inverse tangential longitudinal strain (Ramsay and Huber, 1987), may be active in these layers. In particular, class 3 folds, common in incompetent layers, cannot be produced by the models considered above. In general, when a natural fold cannot be fitted by a combination of the mechanisms considered here, we can infer that other mechanisms have affected the fold development. The method developed in this paper must be improved in the future with the addition of new mechanisms that will have to be mathematically described.

The deformed configuration of the rocks generally does not supply much data on the state of strain, and in most cases the variation of the cleavage orientation through the folded layer is the easiest information to use to fit the geometry of the natural fold with a theoretical fold. Nevertheless, the use of cleavage to obtain principal directions of strain can involve errors. Fortunately, the large number of strain measurements in rocks with primary cleavage suggests that this error is small (see, for instance, Wood, 1974). When a natural fold is fitted by theoretical folds using only information about the geometry of the natural folded layer and the variation of the cleavage orientation, without strain measures, an infinite number of fits exist in many cases, in that fits are possible for any initial thickness ranging between >0 and a maximum value. These fits yield different bulk shortening and the difference between the mechanisms involved in them is mainly in the amount of layer shortening, with the remaining mechanisms undergoing small variations. The $R-\theta$ curves for these fits are also different.

When strain measures in the folded rocks are available, the method enables the selection of the fits with $R-\theta$ curves compatible with the strain data. In this case, every mechanism operates with similar intensity in all the possible fits, and there is a narrow range of initial layer thickness and bulk shortening.

The introduction of area decrease in the pure deformation steps of the models produces fits with higher layer shortening. However, for the most common area decreases in deformed rocks (up to 10%; Wood, 1974; Tan et al., 1995), the variations in layer shortening admitted by the model are small ($<3\%$ in layer shortening increase). Therefore, in most cases, the error linked to the choice of the area change in the models is probably small.

Some errors can be induced in the fit of natural folds due to the difficulty derived from the choice of the guideline, since the assumption that the shape of this line is the average

shape of the bottom and top lines is only an approximation. In addition, the fit of the guideline by a polynomial function is another source of errors. Notwithstanding, small errors in the shape of the guideline produce very small errors in the fit of strain patterns involved in the folding. The identification of the boundaries of a folded layer can also be problematic, because the significance of the boundaries between layers with little lithological contrast is difficult to interpret in terms of folding mechanisms. Another source of problems is given by the lack of a complete knowledge on the original configuration of the natural folded layer. This is obviously a general problem in structural geology that in turn prevents a complete knowledge of the state of strain in folded layers. The fit of folds obtained experimentally or by numerical methods, such as the finite element method, using the analysis here proposed, can be a valuable contribution to the understanding of the kinematics of folding, since in these cases the initial and intermediate stages of the process can be known.

Acknowledgements

The present paper has been supported by the Spanish PB98-1557 project funded by the Ministerio de Educación y Cultura. We are grateful to J. Poblet for many valuable suggestions and to D. Schultz-Ela for his detailed review of the manuscript, which has notably improved the paper. We thank Christine Laurin for her language revision.

References

Anastasio, D.J., Fischer, D.M., Messina, T.A., Holl, J.E., 1997. Kinematics of décollement folding in the Lost River Range, Idaho. Journal of Structural Geology 19, 355–368.

Bastida, F., Aller, J., Bobillo-Ares, N.C., 1999. Geometrical analysis of folded surfaces using simple functions. Journal of Structural Geology 21, 729–742.

Biot, M.A., 1961. Theory of folding of stratified viscoelastic media and its implications in tectonics and orogenesis. Geological Society of America Bulletin 72, 1595–1620.

Biot, M.A., 1965. Mechanics of Incremental Deformations, John Wiley & Sons, New York.

Bobillo-Ares, N.C., Bastida, F., Aller, J., 2000. On tangential longitudinal strain folding. Tectonophysics 319, 53–68.

Chapple, W.M., Spang, J.H., 1974. Significance of layer-parallel slip during folding of layered sedimentary rocks. Geological Society of America Bulletin 85, 1523–1534.

Erslev, E.A., Mayborn, K.R., 1997. Multiple geometries and modes of fault-propagation folding in the Canadian thrust belt. Journal of Structural Geology 19, 321–335.

Fisher, D.M., Anastasio, D.J., 1994. Kinematic analysis of a large-scale leading edge fold, Lost River Range, Idaho. Journal of Structural Geology 16, 337–354.

Fischer, M.P., Jackson, P.B., 1999. Stratigraphic controls on deformation patterns in fault-related folds: a detachment fold example from the Sierra Madre Oriental, northeast Mexico. Journal of Structural Geology 21, 613–633.

Gairola, V.K., 1978. Three-dimensional strain in fold-hinge zone. Tectonophysics 41, 291–319.

Ghosh, S.K., 1996. Refolding by flexural-flow. Journal of Structural Geology 18, 1079–1087.

González-Bonorino, F., 1970. The mechanical factor in the formation of schistosity. 21st International Geological Congress, Copenhagen 18, 303–316.

Groshong, R.H., 1975. Strain, fractures, and pressure solution in natural single-layer folds. Geological Society of America Bulletin 86, 1363–1376.

Gutiérrez-Alonso, G., Gross, M.R., 1999. Structures and mechanisms associated with development of a fold in the Cantabrian Zone thrust belt, NW Spain. Journal of Structural Geology 21, 653–670.

Hobbs, B.E., 1971. The analysis of strain in folded layers. Tectonophysics 11, 329–375.

Hudleston, P.J., Holst, T.B., 1984. Strain analysis and fold shape in a limestone layer and implication for layer rheology. Tectonophysics 106, 321–347.

Hudleston, P.J., Srivastava, H.B., 1997. Strain and crystallographic fabric pattern in a folded calcita vein: the dependence on initial fabric. In: Sengupta, S., (Ed.), Evolution of Geological Structures in Micro-to Macro-scales, Chapman & Hall, London, pp. 259–271.

Hudleston, P.J., Treagus, S.H., Lan, L., 1996. Flexural flow folding: Does it occur in nature? Geology 24, 203–206.

Ramberg, J.G., 1963. Strain distribution and geometry of folds. Bulletin of the Geological Institute of the University of Upsala 42, 1–20.

Ramberg, J.G., 1964. Selective buckling of composite layers with contrasted rheological properties; a theory for simultaneous formation of several orders of folds. Tectonophysics 1, 307–341.

Ramsay, J.G., 1962. The geometry and mechanics of formation of "similar" type folds. Journal of Geology 70, 309–327.

Ramsay, J.G., 1967. Folding and Fracturing of Rocks, McGraw-Hill, New York.

Ramsay, J.G., Huber, M.I., 1987. Modern Structural Geology, Volume 2: Folds and Fractures, Academic Press, London.

Ramsay, J.G., Lisle, R.J., 2000. Modern Structural Geology, Volume 3: Applications of Continuum Mechanics in Structural Geology, Academic Press, London.

Struik, D.J., 1988. Lectures on Classical Differential Geometry, 2nd ed, Dover, New York.

Tan, B.K., Gray, D.R., Stewart, I., 1995. Volume change accompanying cleavage development in graptolitic shales from Gisborne, Victoria, Australia. Journal of Structural Geology 17, 1387–1394.

Tavarnelli, E., 1997. Structural evolution of a foreland fold-and-thrust belt: the Umbria–Marche Apennines, Italy. Journal of Structural Geology 19, 523–534.

Thorbjornsen, K.L., Dunne, W.M., 1997. Origin of a thrust-related fold: geometric vs. kinematic tests. Journal of Structural Geology 19, 303–319.

Treagus, S.H., 1982. A new isogon-cleavage classification and its application to natural folds and model fold studies. Geological Journal 17, 49–64.

Twiss, R.J., Moores, E.M., 1992. Structural Geology, Freeman, New York.

Wood, D.S., 1974. Current views of the development of slaty cleavage. Annual Review of Earth and Planetary Sciences 2, 369–401.